PATENT NOTICE: When Government drawings, specifications, or other data are used for any purpose other than in connection with a definitely related Government procurement operation, the United States Government thereby incurs no responsibility nor any obligation whatsoever and the fact that the Government may have formulated, furnished, or in any way supplied the said drawings, specifications or other data is not to be regarded by implication or otherwise as in any manner licensing the holder or any other person or corporation, or conveying any rights or permission to manufacture, use, or sell any patented invention that may in any way be related thereto.

ASTIA NOTICE: Qualified requestors may obtain copies of this report from the ASTIA Document Service Center, Arlington Hall Station, Arlington 12, Virginia. ASTIA services for the Department of Defense contractors are available through the "Field of Interest Register" on a "need-to-know" certified by the cognizant military agency of their project or contract.

THE UNIVERSITY OF MICHIGAN

4915-1-F

RADC-TDR-63-54

A STUDY OF PLASMA APPLICATIONS IN MICROWAVE CIRCUITS

A. Olte and E. K. Miller

Final Report
4915-1-F

Contract AF 30(602)-2605

January 1963

Prepared for

Rome Air Development Center
Griffiss Air Force Base
Rome, New York

PATENT NOTICE: When Government drawings, specifications, or other data are used for any purpose other than in connection with a definitely related Government procurement operation, the United States Government thereby incurs no responsibility nor any obligation whatsoever and the fact that the Government may have formulated, furnished, or in any way supplied the said drawings, specifications or other data is not to be regarded by implication or otherwise as in any manner licensing the holder or any other person or corporation, or conveying any rights or permission to manufacture, use, or sell any patented invention that may in any way be related thereto.

ASTIA NOTICE: Qualified requestors may obtain copies of this report from the ASTIA Document Service Center, Arlington Hall Station, Arlington 12, Virginia. ASTIA services for the Department of Defense contractors are available through the "Field of Interest Register" on a "need-to-know" certified by the cognizant military agency of their project or contract.

FOREWORD

The invaluable assistance of Kenneth L. Young in designing and fabricating the isolator and carrying out the experiment is gratefully acknowledged. Ronal W. Larson was helpful in suggesting methods for taking the data and contributed considerably in many discussions of the experiments. Chi-Fu Den also assisted in taking the data. The help and support of Ralph E. Hiatt is gratefully acknowledged.

ABSTRACT

An investigation into the potential usefulness of plasmas in microwave structures, with or without a static magnetic field, has been made. Attention has been concentrated on two plasma-microwave configurations.

The RF properties of a coaxial transmission line with a slotted outer conductor which passed through a cylindrical glow discharge were examined. The permittivity of the gas in the line within the discharge chamber could be varied by applying a voltage between the inner and outer conductors, since this determined the extent to which the plasma was drawn into the RF propagation region. The transmission characteristics were examined for a plasma column length of 30.5 cm for frequencies between 500 to 4200 Mc. Argon, helium and nitrogen gas were used at pressures between 0.02 mm Hg and 2 mm Hg. The results are compared with theory using a Lorentzian model to describe the electron motion in the RF field. A graphical technique for finding the electron density and electron momentum transfer collision frequency is discussed and the results compared with Langmuir probe measurements. Operation of the device as a modulator and switch was also investigated. Switching times of 20 to 50 microseconds were obtained with an insertion loss of 2 to 4 db and a power level change of 18 to 20 db.

The second configuration consisted of a plasma slab placed across one side of a square waveguide with its broad side parallel to the waveguide wall. A static

magnetic field is applied normal to the waveguide axis and parallel to the slab. Interaction of a TM_{11} mode with the magneto-plasma was found to be non-reciprocal, with a directivity of 10 db or more attainable over parts of the band between 3 and 4 Gc. The insertion loss was less than 2 db over most of this interval. This behavior was examined as a function of the plasma frequency, magnetic field strength and microwave frequency.

TABLE OF CONTENTS

LIST OF ILLUSTRATIONS

LIST OF ILLUSTRATIONS
(continued)

LIST OF ILLUSTRATIONS
(continued)

LIST OF TABLES

I
INTRODUCTION

One may delineate three areas of interest in the microwave plasma interaction domain which concern the microwave engineers. These are the generation, the amplification, and the control of microwaves by means of plasmas. Under the first topic some research has been done and is continuing on generation of harmonic microwave frequencies by applying very large microwave fields at the fundamental frequency with and without static biasing voltages (Ref. 1.1). Also, it has been recognized that plasmas exhibit instabilities which give rise to oscillations that convert plasma energy into microwave energy at some characteristic frequency. Under the second topic it has been known for some time that the RF signal on an electron beam that is passing through a highly ionized gas will grow when the RF frequency has the proper relation with respect to the plasma frequency (Refs. 1.2 - 1.6). Under the third topic workers have sought to exploit the properties of plasmas in order to accomplish microwave phase shifting and attenuation, both reciprocal and non-reciprocal, switching, and filtering. It is in this area that we have attempted to add to the state of knowledge and the state of the art. Therefore, it may be in order to give a fairly complete bibliography for this area.

Bradley and Pringle (Ref. 1.7) have developed attenuators of the cavity type and of the distributed type which employ the negative glow region of the cold cathode discharge in waveguides as well as in coaxial lines. A number of

attenuation, reflection and absorption curves are provided as a function of the voltages and currents. Starik (Ref. 1.8) has done some further measurements on the attenuation and phase shift of the glow discharge in a rectangular waveguide, the variables being gas pressure and discharge current. Steier and Kaufman (Ref. 1.9) have examined the coupling between two separate rectangular waveguides that are running parallel and are connected by a transverse plasma column through their narrow walls, with the column outside the guide enclosed in a round metal pipe. By varying the discharge current one may vary the coupling between the guides. A different directional coupler has been tested by Willis (Ref. 1.10) in which a section of the common wall between two waveguides has been removed and replaced by a discharge tube. The degree of coupling is controlled by the discharge current. Kaufman and Steier (Ref. 1.11) have recently investigated a microwave filter which employs the Tonks-Dattner resonance of a plasma column in order to provide a coupling between two waveguides. The rectifying properties of a conical cold cathode have been shown by Walsh (Ref. 1.12) to have potential usefulness for microwave power monitoring purposes. Considerable work (Ref. 1.13) has been done to exploit the current derived from secondary emission (the so-called multipactor discharge) for nanosecond switching of high power microwaves.

The formal objectives of this contract include the theoretical and experimental investigation of microwave structures which contain plasma, with or without

dc magnetic field present, and the use of such structures in practical microwave components. In this we have attempted to strike a balance between the immediate and pressing need of a practical and useful device and the long range goal of fully understanding plasmas which is so essential to successful applications.

In Section II we report on our investigation of the microwave properties of helium, argon, and nitrogen gas discharges.[+] This involved the use of a glow discharge which was created between a slotted cylindrical shell and an enclosing shell. The slotted cylinder formed the outside wall of a coaxial waveguide. By applying a voltage between the conductors of the coaxial line one could draw the plasma from the glow discharge further into the coaxial line, or reject it. Considerable study was carried out on the microwave properties of such plasmas as a function of gas pressure, type of gas and discharge voltages. Some of these measurements were compared with simultaneous Langmuir probe measurements. Particular emphasis was placed on finding regions of operation where the device would have some promise as either an attenuator, modulator or a switch. In addition, attempts were made to vary the plasma in the interaction region by ionization as well as by diffusion processes. It appears that the latter process does not hold much promise.

So far we have mentioned only work done on isotropic plasmas. By impressing a static magnetic field on the plasma we obtain an anisotropic medium which has a much more complicated behavior than that discussed so far. The

+ A preliminary report of this work is contained in Trans. IEEE, PTGNS, Vol. NS-10, January 1963.

ionosphere in the presence of the earth's magnetic field is such a medium, and therefore it is not surprising that in this context the first Magneto-Ionic theory was worked out to account for the observed electromagnetic propagation effects. These representations are simple and have gained wide acceptance and use notwithstanding the fact that considerably more complete, but much more complicated and cumbersome theory is available today. The elementary Magneto-Ionic theory has been well summarized by Ratcliffe (Ref. 1.14). If a uniform magnetostatic field is applied in the x-direction to a uniform and neutral plasma then the permittivity tensor according to this theory assumes the form

$$(\epsilon) = \begin{pmatrix} \epsilon^o & 0 & 0 \\ 0 & \epsilon & j\kappa \\ 0 & -j\kappa & \epsilon \end{pmatrix} \tag{1-1}$$

where

$$\epsilon^o = \epsilon_o \left(1 + \frac{1}{j\omega} \frac{\omega_p^2}{\nu_m + j\omega}\right),$$

$$\epsilon = \epsilon_o \left(1 + \frac{1}{j\omega} \frac{\omega_p^2 (\nu_m + j\omega)}{(\nu_m + j\omega)^2 + \omega_H^2}\right)$$

$$\kappa = j \frac{\omega_H}{\omega} \frac{\omega_p^2}{(\nu_m + j\omega)^2 + \omega_H^2},$$

and ω_p, ω_H, ω and ν_m are the plasma frequency, gyromagnetic (cyclotron) frequency, microwave frequency, and effective momentum transfer collision frequency

respectively. The permeability is essentially that of free-space, i.e., $\mu = \mu_o$. The electromagnetic plane waves that may propagate in such media that is infinite in extent are well understood.

It is well known that ferrites in a magnetostatic field are anisotropic and have found wide applications in microwave components (Ref. 1.15). The permeability tensor, with a magnetostatic field in the x-axis direction, is, in the lossless approximation, given as

$$(\mu) = \begin{pmatrix} \mu_o & 0 & 0 \\ 0 & \mu & j\kappa \\ 0 & -j\kappa & \mu \end{pmatrix} \qquad (1\text{-}2)$$

where

$$\mu = \mu_o \left(1 + \frac{\omega_o^2 \chi_o}{\omega_o^2 - \omega^2}\right)$$

$$\kappa = \mu_o \frac{\omega \omega_o \chi_o}{\omega_o^2 - \omega^2}$$

ω_o is the gyromagnetic frequency and χ_o is the magnetostatic susceptibility. The permittivity, ϵ, of a magnetized ferrite is essentially isotropic. One notices that the respective tensors for gyromagnetic media and the magneto-ionic media are of the same form. (Obviously this does not imply that the frequency dependence of the corresponding tensor components is identical.) This means that the gyromagnetic media is an analog, in a certain sense, of the magneto-ionic media. One would

therefore expect to do similar things with the magneto-ionic media in waveguide structures that we now achieve with ferrites. For example, by judiciously selecting the optimum waveguide and plasma structures, one should be able to produce microwave phase shift and attenuation under reciprocal and non-reciprocal conditions. Some experimental and theoretical work has already been done on coaxial magneto-ionic phase shifters (Refs. 1.16 and 1.17).

The operation of some of these devices is deduced by perturbation analysis that uses the plane wave solutions. Therefore, it is constructive to visualize the transformation connecting the plane waves in gyromagnetic media with those in magneto-ionic media. This transformation follows readily from the similarity of the (ϵ) and (μ) tensors and the symmetries between the $\overline{E}$ and $\overline{H}$ fields that are exhibited in Maxwell's equation. For example, if we have found the plane wave solutions for $\overline{E}$ and $\overline{H}$ in a gyromagnetic media (medium of infinite extent is naturally implied) and have studied the physical implications of these plane waves, then we may obtain the corresponding equations (and also some of the physical insight by implication) of the magneto-ionic media by the following simple transformation:

$$\begin{aligned} (\mu) &\longrightarrow (\epsilon) \\ \epsilon &\longrightarrow \mu_o \\ \overline{E} &\longrightarrow -\overline{H} \\ \overline{H} &\longrightarrow \overline{E} \end{aligned} \qquad (1\text{-}3)$$

These transformations are valid only for waves in an infinite medium, and do not apply to waveguide modes, for example, because boundary conditions also have to be considered.

The ferrite resonance isolator in a rectangular waveguide which employs the TE_{10} mode is very common. The direct analog in the plasma case would employ the TM_{10} mode. The transformation implies that for this mode the normal component of the electric field is zero and the tangential component is maximum on the waveguide wall. We know that such a mode does not exist in common waveguides. The next mode which is suitable and does exist is the TM_{11} mode. We have constructed and tested a plasma cyclotron resonance isolator which employs the TM_{11} mode. The results of this study and the pertinent analysis is presented in Section III.

From the foregoing account, no doubt incomplete, it is clear that considerable attempts have been made to introduce plasmas, with and without magnetostatic fields, into the microwave technology. However, it is probably true that only in two instances have plasmas found widespread application: that is in TR tubes for microwave duplexers and as noise sources for microwave receiver calibration. Anyone trying to exploit magneto plasmas in microwave component technology meets the proven and well-established capability of ferrites head-on. To successfully exploit microwave plasma devices one must offer, as an end result, not something equal to the ferrite device, but something considerably better than what is available in present day microwave ferrite and semi conductor technology.

The main advantage of the plasma device could be that its properties may be varied, or it may be turned off altogether. Ferrites and semiconductors, once made, are relatively immutable, but they are stable. Plasmas currently used change with respect to time, because the discharge gas interacts with the cathode surfaces and the walls of the container. Cathodeless discharges help to obviate some of these difficulties, but create others in turn. The usual ionizing source is of high frequency, and thus is relatively expensive, and some instabilities result from attempts to couple the ionizing microwave power into the plasma. This leaves the thermal plasmas and both cold and hot cathode discharge plasmas for consideration. The former involves the maintenance of very hot filaments and chemically corrosive gases such as cesium, for example, at a controlled pressure. The cathode discharge plasmas are easier to obtain, but in the present state of technology they produce low frequency oscillations and are rather unstable as to the discharge properties. It does appear that the present state of the art in production and containment of plasmas for microwave circuit component application is not competitive with alternative designs available. This does not necessarily deny some future use for plasmas in microwave circuitry. Plasmas have been receiving attention only very recently and they are much more difficult to understand and analyze than solids, because we are dealing with a medium in which the interactions are neither weak nor strong, but of intermediate value. It is equally true that simple theories such

as the magneto-ionic theory of the ionosphere are not adequate to evaluate the future of plasmas or to predict the best applications of plasmas in microwave circuits. In addition to the objective of designing microwave circuit components containing plasmas, there must also be applied research leading to delineation of areas where plasmas may be able to complement, extend, or supplant present and future solid state materials.

REFERENCES FOR SECTION I

1.1 J. R. Baird and P. D. Coleman, "Frequency Conversion in a Microwave Discharge", Proc. IRE, Vol. 49, No. 12, 1890-1900(Dec. 1961).

1.2 Z. S. Chernov and G. A. Bernashevski, "Amplification of Microwaves by Means of Plasma," Proc. Symp. Electromagnetics and Fluid Dynamics of Gaseous Plasma, New York. Polytechnic Press of P. I. B., New York, 31-35(1961).

1.3 K. J. Kislov and E. V. Bogdanov, "Interaction Between Slow Plasma Waves and an Electron Stream," Proc. Symp. Electromagnetic and Fluid Dynamics of Gaseous Plasma, New York. Polytechnic Press of P. I. B., New York, 249-268(1961).

1.4 G. F. Freire, "Interaction Effects Between a Plasma and a Velocity-Modulated Electron Beam," W. W. Hansen Laboratory of Physics, Stanford University, Report No. 890 (AFCRL 62-82)(Feb. 1962).

1.5 M. A. Allen, P. Chorney and G. E. St. John, "Beam Plasma Interaction Experiments in the X-band," NEREM Record, 186-187(1962).

1.6 H. Groendijk, "Amplification by Longitudinal Waves in Beam-Plasma Systems," NEREM Record, 184-185(1962).

1.7 E. M. Bradley and D. H. Pringle, "The Theory and Design of Gas-Discharge Microwave Attenuators," J. British IRE, XV, (New Series), 11-24 (1955).

1.8 A. M. Starik, "Propagation of Microwave Oscillations in a Waveguide Containing the Cathode Parts of a Glow Discharge," Radio Eng. and Elec. Phys. (Soviet), No. 9, 1365-1371(Sept. 1961).

1.9 W. H. Steier and I. Kaufman, "A Plasma Guide Microwave Selective Coupler," IRE-PGMTT, Vol. 9, 499-506(Nov. 1961).

1.10 J. Willis, "A Plasma Controlled Directional Coupler," IRE-PGMTT, Vol. 10, No. 5, 383-389(Sept. 1962).

1.11 I. Kaufman and W. H. Steier, "A Plasma-Column Band-pass Microwave Filter," IRE-PGMTT, Vol. MTT-10, No. 6, 431-439(Nov. 1962).

1.12 D. Walsh, "A New Type of Cold Cathode Microwave Power Monitor Diode," Microwave J., Vol. 5, No. 12, 26(1962).

1.13 C. Milazzo, "Microwave High-Power Nanosecond Switch Using Multipactor Discharge," Microwave J., Vol. 5, No. 3, 93-98(March 1962).

1.14 J. A. Ratcliffe, The Magneto-Ionic Theory and Its Applications to the Ionosphere, Cambridge University Press, pg. 184 (1959).

1.15 B. Lax and K. J. Button, Microwave Ferrites and Ferrimagnetics, McGraw-Hill Book Company, New York (1962)

1.16 H. Bandel, A. Penico and F. Olsen, "Investigation of the Use of Electron Cyclotron Resonance to Obtain Microwave Phase Shift", Microwave Physics Laboratory, Sylvania Electronic Products Scientific Report No. 1, ASTIA Document No. AD 152391 (1958).

1.17 E. F. Tubbs, "Investigation of the Use of Electron Cyclotron Resonance to Obtain Microwave Phase Shift," Microwave Physics Laboratory, Sylvania Electronic Products, ASTIA Document No. AD 214421 (March 1959).

II

COAXIAL PLASMA ATTENUATOR

2.1 Introduction

Our work done on extending plasma-microwave interaction studies to coaxial configurations is reported in this section. It is natural to divide the section into two parts. The first part is a general study of wave propagation in a coaxial glow discharge. The experimental design of the apparatus and the associated circuitry are discussed in detail. The results on the gases studied are presented and analyzed. After establishing the optimum plasma operating conditions for the RF attenuation a new grid was constructed. The RF modulation experiment carried out with this modification is reported in the second part of this chapter.

2.2 Wave Propagation in a Coaxial Glow Discharge

Glow discharge was investigated from the viewpoint of obtaining a low loss plasma which may be varied in some desired manner to control the microwaves. Plasma frequencies and momentum transfer collision frequencies were obtained for helium, argon and nitrogen.

The adequacy of the Lorentzian plasma model was tested for some range of parameters. The plasma frequency and the momentum transfer collision frequency were obtained from the transmission loss measurement at two different microwave frequencies. In addition to the electron temperature the plasma frequency was also obtained from Langmuir probe measurements. The plasma

frequencies obtained by the two methods did not agree as consistently as reported by Nicoll and Basu (Ref. 2.1). By reasonable assumptions in the theory the momentum transfer collision probability has been computed from the measured data and compared with the collision probability obtained by other investigators using the electron beam method.

The experiment is described in the following section where also the experimental techniques are presented and analyzed. The last section contains the data and its critical evaluation.

2.2.1 The Experiment

2.2.1.1 Experimental Set-up

The experimental arrangement consists of a rigid 50 ohm coaxial transmission line, the central portion of which is a 30.48 cm (12 inch) long cage line, located axially within a cylindrical vacuum chamber of 3.5 inch inside diameter and 16 inch length. The inside wall of the vacuum chamber serves as the cathode for a glow discharge taking place between it and the 8 rods forming the outside conductor of the cage line, hereafter called the grid. The center conductor of the transmission line, hereafter called the anode, may have a variable voltage applied between it and the grid. In Figure 2.1 is shown the discharge chamber along with the associated microwave components.

Circular plates of ordinary window glass, 1/2 inch thick and 5.470 inches in diameter form the end walls of the chamber. The coaxial line passes through a

concentric 1.360 inch diameter hole in the glass end-plates. The glass-metal interfaces at the edge of the glass and the center hole are sealed with "O" rings, while a tapered teflon bead seals the transmission line. Figure 2.2 shows the axial cross section of one of the two identical ends of the chamber. Figure 2.3 is a cross section of the system normal to the axis showing the relation between the cathode, grid and anode. Three ports are located in the chamber wall for the connection of the vacuum pump, the gas inlet and one spare. The vacuum gauge was later connected to the system through a hole drilled in the outer conductor of one of the RF feed-throughs.

The chamber is constructed from a brass cylinder with 1/4 inch walls. The inside surface of the chamber is coated with a 0.003 inch nickel surface deposited by electroplating. Nickel is also used for the center conductor of the transmission line within the chamber, while the grid rods are of stainless steel. Two stainless steel rings 0.732 inch inside diameter, through which the grid rods pass, are located 4 inches from each end of the cage section. These were required to keep the grid rods from distorting. All other parts of the chamber are of brass.

Two 1/8 inch copper tubes for cathode cooling water are wound in parallel around the chamber. Over this are crossed two coils of 48 turns and 1382 turns of No. 20 wire and a 1468 turn coil of No. 14 wire. Three 1/8 inch diameter copper tube layers are buried half-way through the coil for cooling.

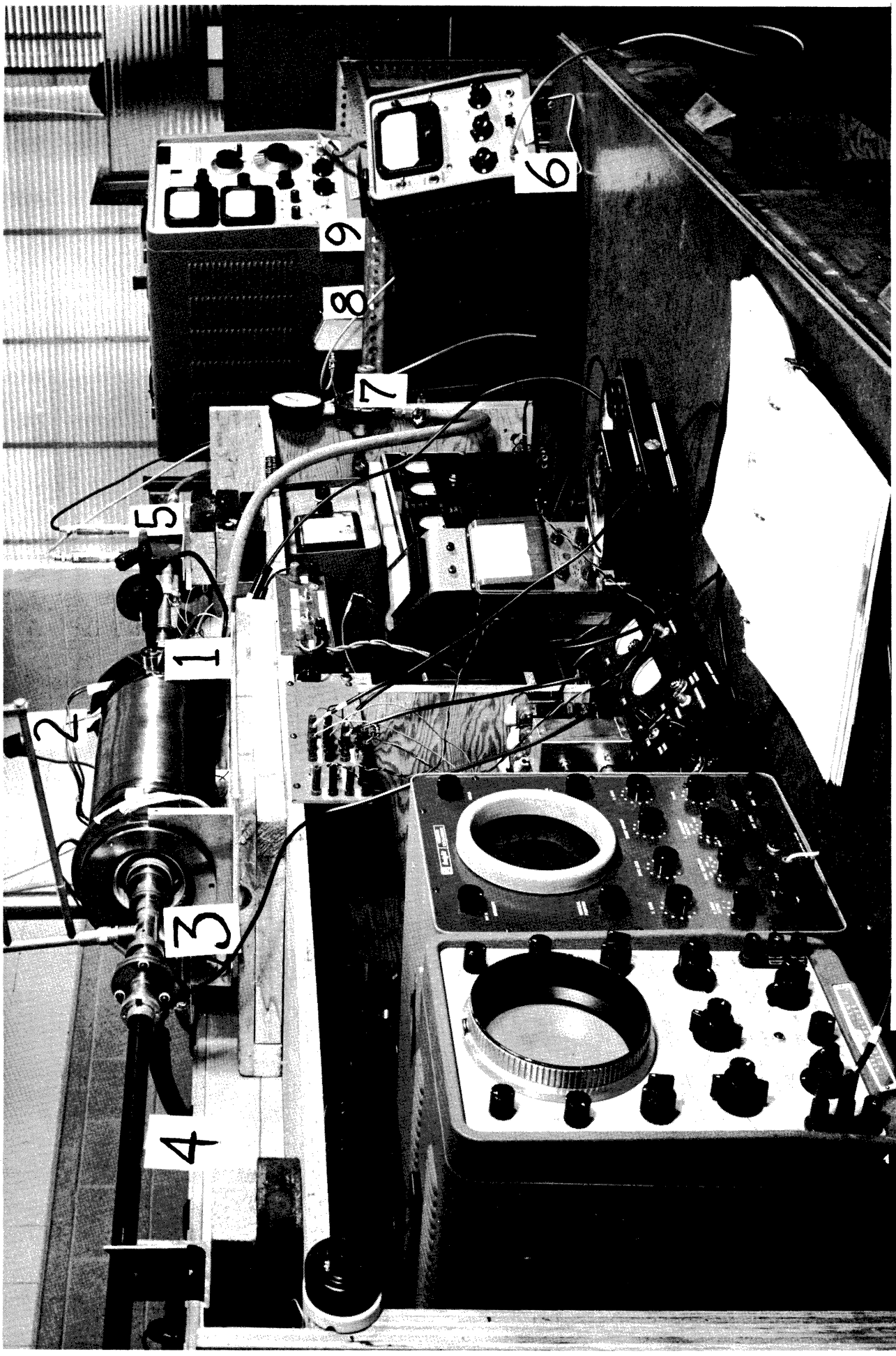

FIGURE 2.1: A VIEW OF THE APPARATUS: (1) VACUUM CHAMBER, (2) VACUUM GAUGE SENSING ELEMENT, (3) TRANSMITTED POWER SAMPLER, (4) RF MATCHED LOAD, (5) DIRECTIONAL COUPLER, (6) SWR METER, (7) "VACUUM REGULATOR, (8) SWITCH FOR FORWARD, REFLECTED AND TRANSMITTED POWER, (9) RF GENERATOR.

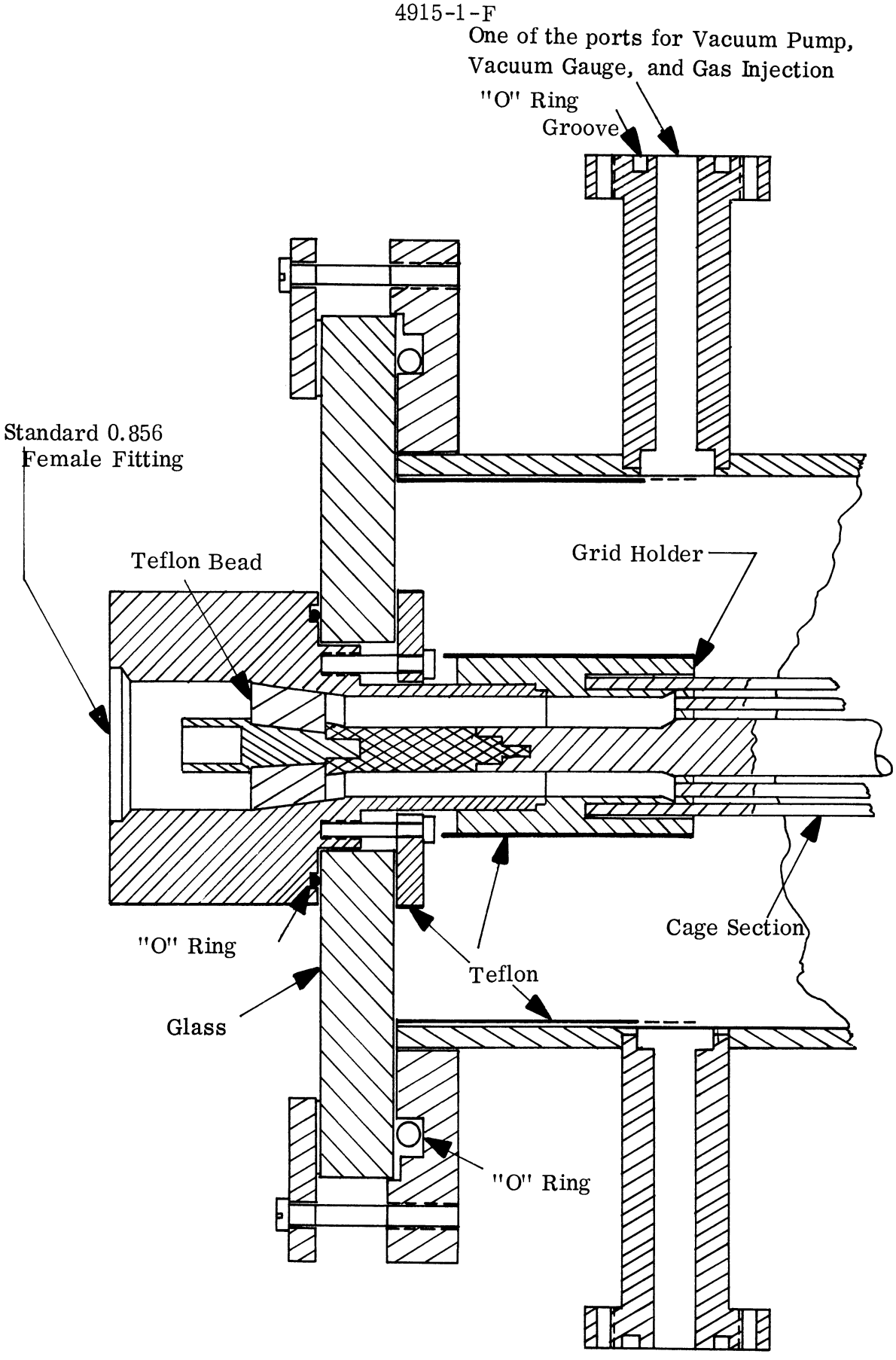

FIG 2.2: CROSS SECTION OF ONE OF TWO IDENTICAL ENDS OF THE CHAMBER

The external RF circuit is shown in the block diagram of Figure 2.4. A type N dc center block for the frequency range 100 to 4000 Mc is connected to a constant impedance transition from a type N to 0.856 inch outside diameter coaxial line. This is followed by an outside dc blocking capacitor which connects directly to the chamber input (both inputs are standard 0.856 inch female fittings). Maintaining a constant impedance, the line tapers to a 0.716 inch outside diameter passing through the tapered 1/2 inch thick teflon seal. The center conductor is undercut passing through the teflon. A taper was used for the teflon seal in order to have greater mechanical strength and a more positive vacuum seal. The line then tapers to an equivalent outside conductor diameter of 0.808 inches at the transition to the cage section.

The cage line was designed on the basis that the outside conductor of a coaxial line may be replaced by a grid of 2n conductors. This problem is discussed by King (Ref. 2.2). If the radius of the grid conductors is a and the centers of the grid conductors are on radius b, then $a = b/2n$ where b is also the radius of the former solid cylinder. The cage dimensions were chosen such that the impedance would be 50 ohms. Figure 2.3 shows the cage dimensions.

At the output end, a 0.856 inch cylinder with a 1.33 cm x 0.305 cm slot, through which a sampling probe is passed serves as a transmitted signal sampler. Magnetic coupling was chosen for the probe because it gave a flatter coupling, as a

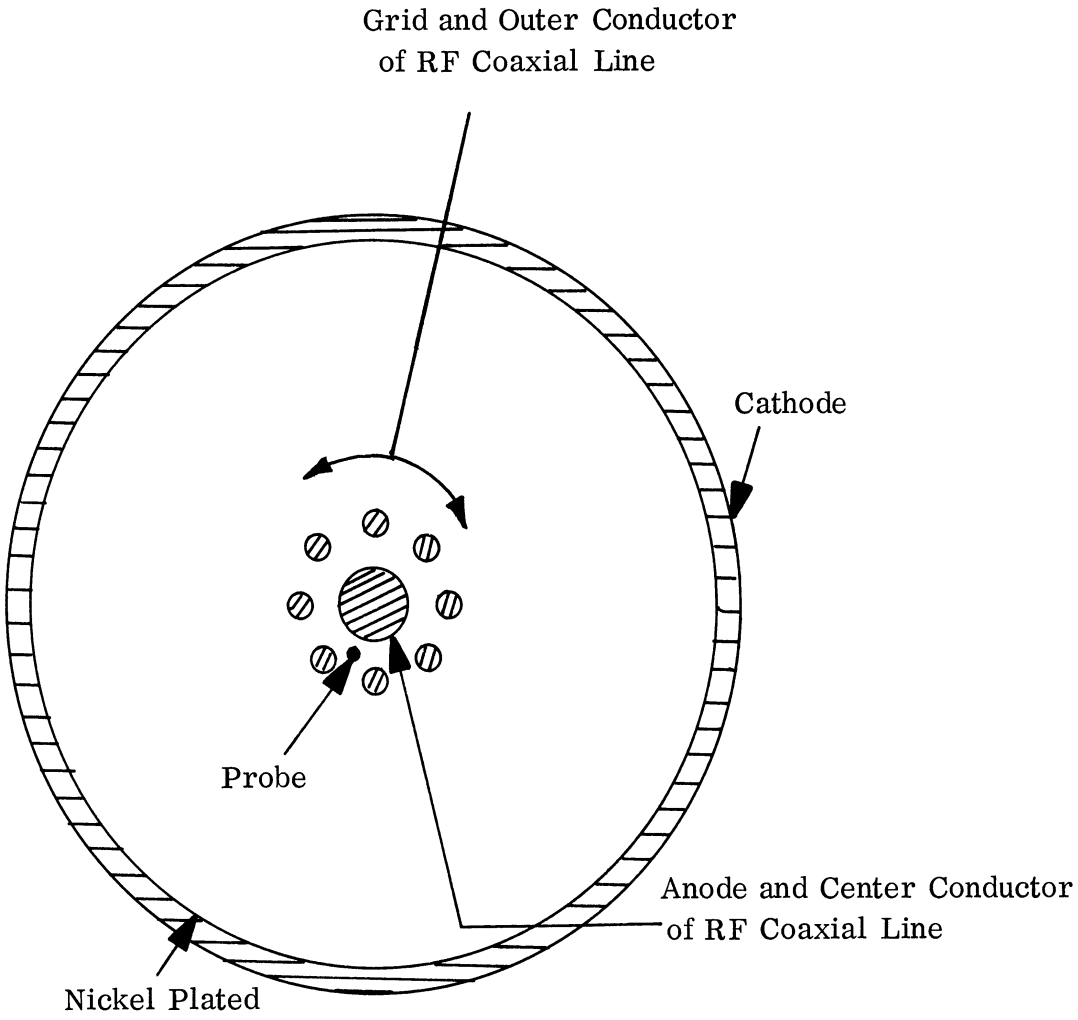

Cathode Diameter (inside): 8.88cm
Anode Diameter: 0.896cm
Grid Rod Diameter: 0.257cm
Grid Circle Diameter: 2.05cm

FIG. 2.3: CROSS SECTION THROUGH CAGE SECTION NORMAL TO AXIS

function of frequency than capacitive coupling. The size of the magnetic coupling loop was selected to give a maximum of -26 db coupling at 500 Mc and -17.5 db at 2000 Mc. The coupling could be adjusted by varying the probe penetration. Another outside dc block follows, across which the grid-anode voltage is applied. The line is terminated by matched RF load (less than 1.10 VSWR between 700 and 4000 Mc) which is at the same time a dc short.

The VSWR of the cage section only was measured with a slotted line. It was found to be < 1.2 from 700 to 3000 Mc and < 1.5 from 3000 to 4200 Mc. No appreciable difference was found in the VSWR when an aluminum foil was wrapped around the grid. The VSWR of the entire set-up as shown in Figure 2.4 was measured with a slotted line and found to be < 1.6 from 500 to 4200 Mc for the usual probe coupling values used during an experiment.

The measured net pumping rate in our system is 0.253 liters/second at 1.0 mm and 0.185 liters/second at 0.1 mm Hg. The ultimate pressure is between 0.001 and 0.010 mm Hg. The connection of the inlet gas lines, the vacuum gauge and the pump is shown in Figure 2.5.

A high pressure regulator on the bottle was set to keep the pressure between 20 to 25 psi absolute in the line feeding the "vacuum" regulator. A "vacuum" regulator reduced this pressure down to 50 mm Hg. With the pump on and the "exit valve" fully open the gas pressure in the chamber was easily adjusted with the "leak

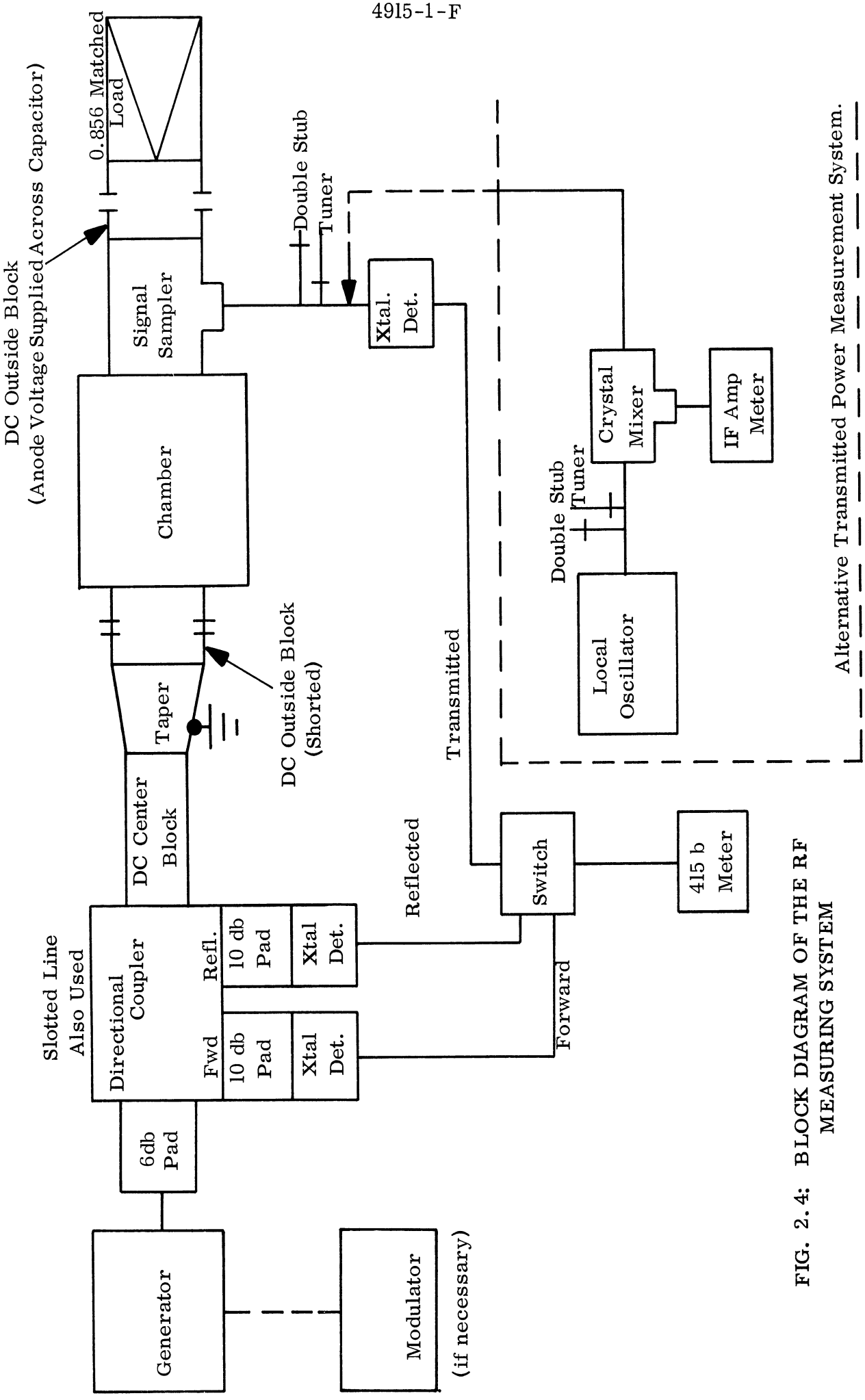

FIG. 2.4: BLOCK DIAGRAM OF THE RF MEASURING SYSTEM

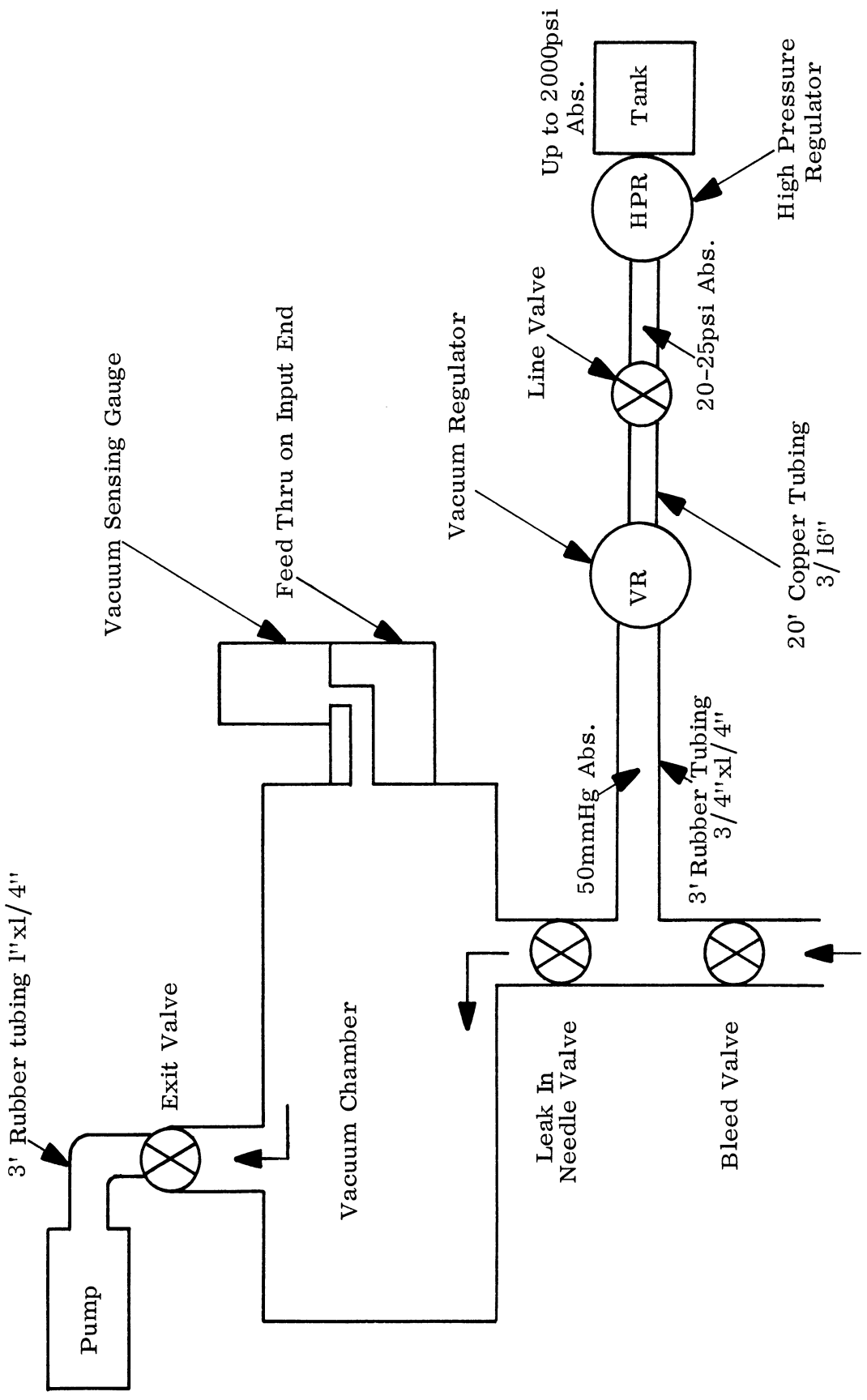

FIG. 2.5: DIAGRAM OF GAS SYSTEM SHOWING ARRANGEMENT OF REGULATOR, FEED LINES AND VACUUM CHAMBER

in needle valve" to the desired value. The line between the vacuum chamber and the "vacuum" regulator was regularly pumped out to keep the gas contamination at a minimum.

The vacuum gauge (Magnevac) is a thermal conductivity type gauge, in which the filament is kept at a constant temperature regardless of pressure and the power thus required is an indication of the pressure. The gauge was calibrated for the three gases used in this experiment; nitrogen, argon and helium. The agreement with a McLeod gauge (Flosdorff modification) was very good for nitrogen, but for helium, the Magnevac gauge read about 38 per cent high from 0.070 to 0.7 mm Hg pressure, with the difference increasing rapidly beyond that point. For argon, the measured pressures were less than the true pressure by 20 per cent at 0.100 mm Hg and 50 per cent at 1.00 mm Hg, with the difference increasing for higher pressures.

Some problems were encountered with leaks through the teflon beads and around two of the side ports where they are soldered to the chamber. They were located with a helium leak detector and successfully closed with glyptol. No effect on the RF reflections was noticed after applying the glyptol to the beads.

2.2.1.2 Discharge Characteristics

A discharge cathode current of usually between 100 ma and 600 ma was used when taking the RF data, depending upon the gas and the pressure. The circuit used

to operate the discharge is shown in Figure 2.6. This includes the anode, cathode and probe supplies, with their respective metering arrangements.

For purposes of analyzing the RF data, or at least interpreting it, it is desirable to operate the discharge with the entire cathode emitting uniformly, or perhaps in the abnormal glow region, so that the grid receives a uniform current. Although this condition may be somewhat established by visual observation, a graph of the cathode discharge voltage-current curve was used to verify it. Teflon sleeves were wrapped around the grid holder and cathode ends to confine the discharge to the cage section.

The discharge stability was the most difficult problem to cope with in operating this experiment. It can be broken down into two general categories: various abnormal glow conditions and arcing, and a changing cathode discharge current at a constant pressure and voltage. Arcing occasionally took place between the grid holders and the cathode surface. The abnormal glow took the form of a discharge between the grid and the gas inlets and outlets, and various localized spots of brighter than surrounding glow on the grid and between grid and anode. A slow decrease in cathode current from its initial value when the glow was turned on, by as much as 50 per cent in a period of a half-hour was characteristic of nitrogen. Argon and helium generally gave a rapid decrease in cathode current of about 10 per cent after the glow was initiated, and then remained fairly steady.

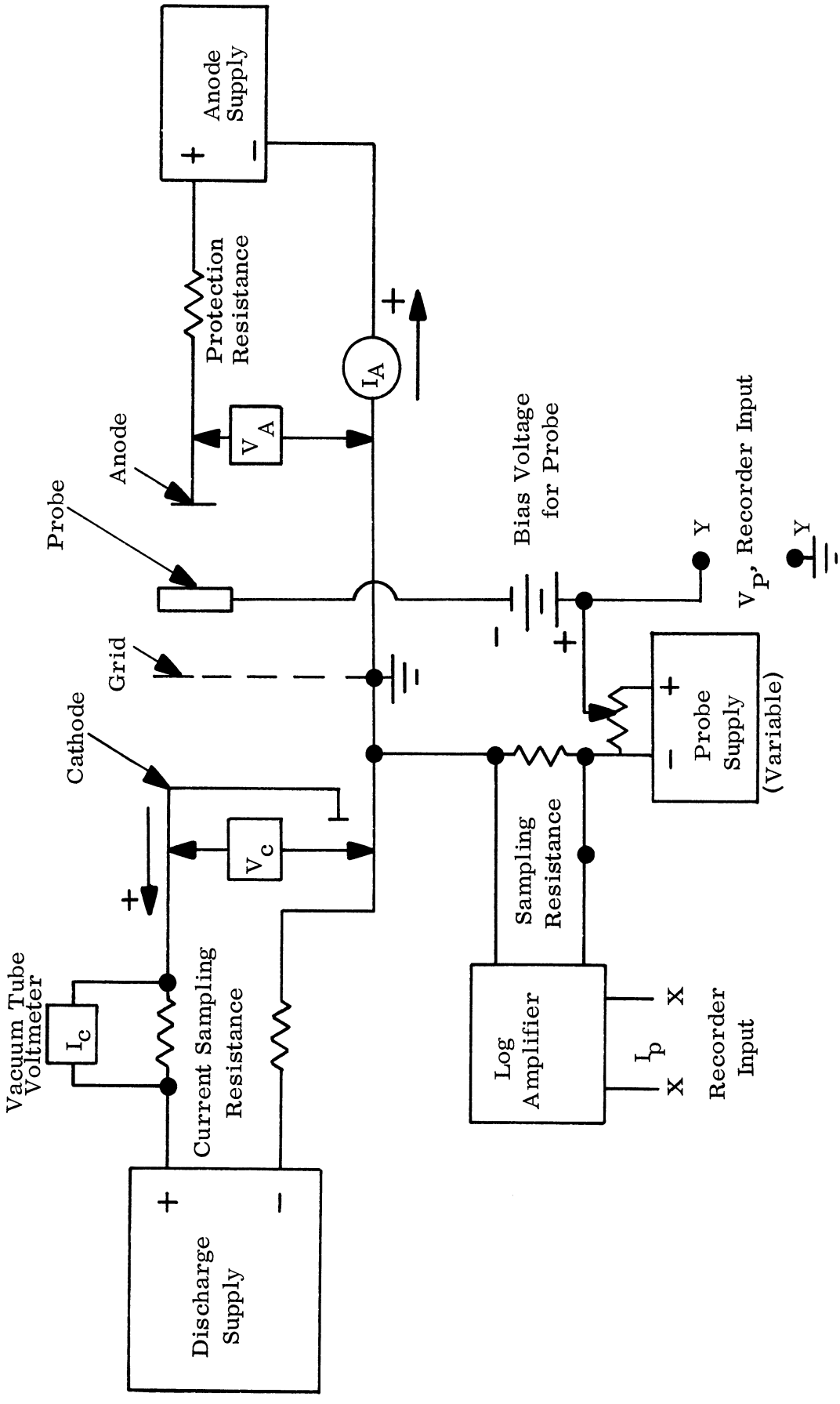

FIG. 2.6: CATHODE, ANODE AND PROBE SUPPLY CIRCUITS AND METERING ARRANGEMENTS

In appearance, the argon discharge was blue in color, the helium a lighter blue and the nitrogen a violet-purple. At a pressure of about 0.5 mm Hg and lower for nitrogen and argon, the discharge had the form of a cylinder of glowing gas, quite uniform in appearance, surrounding the grid-anode region. It was quite clearly separated from the cathode by a dark region. Helium took on this appearance at a pressure of about 2 mm. When the anode was conducting, a visible brightening of the discharge was noticeable, in the cylindrical region.

2.2.1.3 Basic RF Measurements

The external RF circuit (Figure 2.4) is set up for measuring the reflection coefficients by means of either a directional coupler, or a slotted line, and the power transmission coefficient (PTC) with respect to no discharge, using an incident TEM wave of about 1 mw power. Two methods were used to measure the transmitted power: 1) a crystal detection system using 1000 cps modulation on the RF input wave and a Hewlett-Packard 415B SWR meter; 2) a heterodyne system using a local oscillator, a mixer, and a 30 Mc IF amplifier. The former system was used when the transmission losses did not exceed 30 db. The heterodyne system was employed for measurements where the transmission loss exceeded 30 db. We were able to measure a PTC as low as -80 db with this arrangement, but it was somewhat more inconvenient to use. Both systems are considered accurate to at least 2 per cent of the reading in db.

In appearance, the argon discharge was blue in color, the helium a lighter blue and the nitrogen a violet-purple. At a pressure of about 0.5 mm Hg and lower for nitrogen and argon, the discharge had the form of a cylinder of glowing gas, quite uniform in appearance, surrounding the grid-anode region. It was quite clearly separated from the cathode by a dark region. Helium took on this appearance at a pressure of about 2 mm. When the anode was conducting, a visible brightening of the discharge was noticeable, in the cylindrical region.

2.2.1.3 Basic RF Measurements

The external RF circuit (Figure 2.4) is set up for measuring the reflection coefficients by means of either a directional coupler, or a slotted line, and the power transmission coefficient (PTC) with respect to no discharge, using an incident TEM wave of about 1 mw power. Two methods were used to measure the transmitted power: 1) a crystal detection system using 1000 cps modulation on the RF input wave and a Hewlett-Packard 415B SWR meter; 2) a heterodyne system using a local oscillator, a mixer, and a 30 Mc IF amplifier. The former system was used when the transmission losses did not exceed 30 db. The heterodyne system was employed for measurements where the transmission loss exceeded 30 db. We were able to measure a PTC as low as -80 db with this arrangement, but it was somewhat more inconvenient to use. Both systems are considered accurate to at least 2 per cent of the reading in db.

Preliminary measurements were taken with the cathode grounded, but the noise problem encountered with the whole RF line floating above ground led us to modify our equipment so that the grid could be operated at ground potential. For this reason, the vacuum gauge sensing element was shifted from one of the side ports to one of the feed-through pieces, having access to the chamber through a 0.25 cm hole, about 4 cm long. The outside dc block at the input to the chamber was left connected, but shorted out.

The high pressure operating limit was determined primarily by the apparent plasma inhomogeneities in the grid-anode space; the low pressure limit by the small cathode current and the length of the electron mean-free path (MFP). The MFP for electrons of 1 ev energy in argon, helium and nitrogen respectively, at 1.0 mmHg, and the gas temperature of 320^{o}K are 0.24 cm, 0.059 cm, and 0.039 cm. The MFP is inversely proportional to pressure. RF data was generally taken between 0.09 mm and 2 mm Hg.

In order to be able to analyze the RF data which is obtained, some assumptions must be made about the characteristics of the plasma, and a suitable model chosen to describe its RF properties. If one can use the Lorentzian model to take into account the effect of elastic collisions of electrons with the gas molecules and if the plasma is uniform, then, from the electron equation of motion one obtains the permittivity

$$\epsilon = \epsilon_o \left(1 - \frac{f_p^2}{f\left(f - j\,\frac{\nu_m}{2\pi}\right)}\right), \qquad (2\text{-}1)$$

where f is the electromagnetic frequency, ν_m the momentum transfer collision frequency and f_p the plasma frequency, given by

$$f_p = \sqrt{\frac{N q^2}{4\pi^2 \epsilon_o m}} \tag{2-2}$$

with N, q, and m the number density, charge and mass, respectively, of electrons and ϵ_o the permittivity of vacuum. The propagation constants inside and outside the plasma are $k = 2\pi f \sqrt{\mu_o \epsilon}$ and $k_o = 2\pi f \sqrt{\mu_o \epsilon_o}$, respectively. The permeability of the medium is μ_o. A dielectric constant $K = (k/k_o)^2 = \epsilon/\epsilon_o$ could be used to represent the plasma. Making use of appropriate boundary conditions one may solve for the reflected and transmitted plane wave amplitudes in terms of k_o, k, K and plasma length ℓ. For unit amplitude incident wave the amplitudes of the transmitted and reflected waves are the voltage transmission and reflection coefficients,

$$\tau = \frac{4\sqrt{K}\, e^{jk_o\ell}}{(1+\sqrt{K})^2 e^{jk\ell} - (1-\sqrt{K})^2 e^{-jk\ell}} \tag{2-3}$$

$$\Gamma = \frac{(1-K)(e^{jk\ell} - e^{-jk\ell})}{(1+\sqrt{K})^2 e^{jk\ell} - (1-\sqrt{K})^2 e^{-jk\ell}}, \tag{2-4}$$

respectively. The power transmission and reflection coefficients are the respective voltage coefficients squared.

A series of measurements of the power transmission coefficient were made for argon, helium and nitrogen for several values of gas pressure, cathode current and anode current over the frequency range between 500 and 4200 Mc. Some typical curves showing these results are given in Figs. 2.7, 2.8 and 2.9. There are two curves on each graph, one for an anode potential of -150 volts with respect to the grid (Case 1), the other for the maximum value of anode current used in the experiment (Case 2). I_{co} is the cathode current drawn by the discharge with the anode circuit open. If the plasma properties may be described by the Lorentzian model and there is a radial uniformity of the plasma, then with the proper choice of f_p and ν_m, one should be able to obtain a theoretical curve using (2-3) that does fit the experimental curve reasonably well. The solid lines in Figs. 2.7 - 2.9 are theoretical curves calculated using a plasma frequency and collision frequency obtained from the corresponding experimental data of Case 2.

While the agreement seems acceptable in the frequency range 1200 - 4200 Mc, there is an increasing amount of discrepancy between the theoretical and experimental curves for the lower frequencies. This is especially the case for the argon and helium data between 500 and 700 Mc, where the experimental data exhibits a sharp upswing. No theoretical curves are included for the -150 volt case, where a band absorption phenomena is apparently occurring, particularly for argon and helium. Some preliminary theoretical analysis using a two-layer region to allow

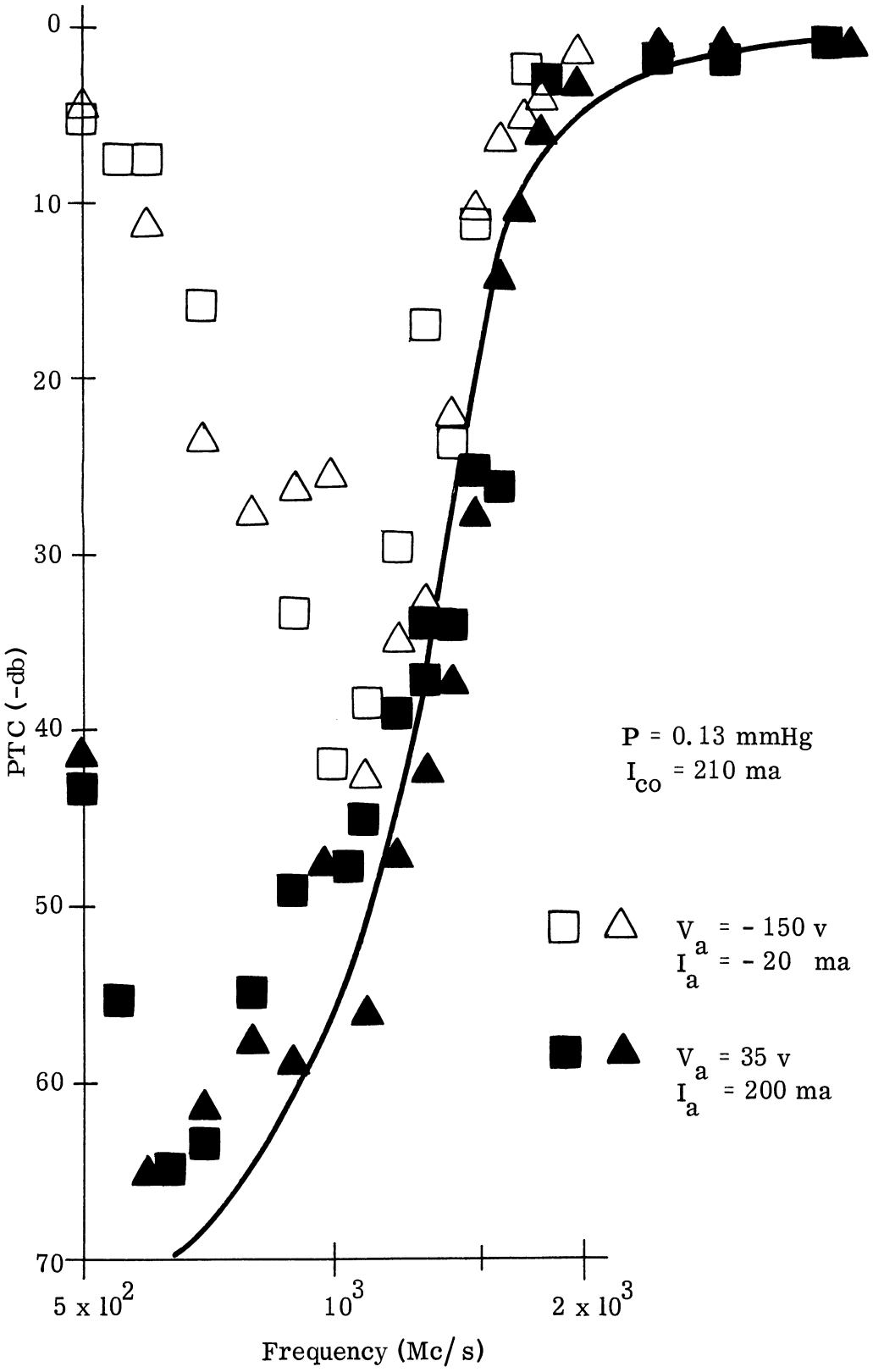

FIG. 2.7: POWER TRANSMISSION COEFFICIENT VS FREQUENCY IN ARGON DISCHARGE. SOLID LINE IS THEORETICAL CURVE FOR f_p = 1500 Mc and ν_m = 200 Mc.

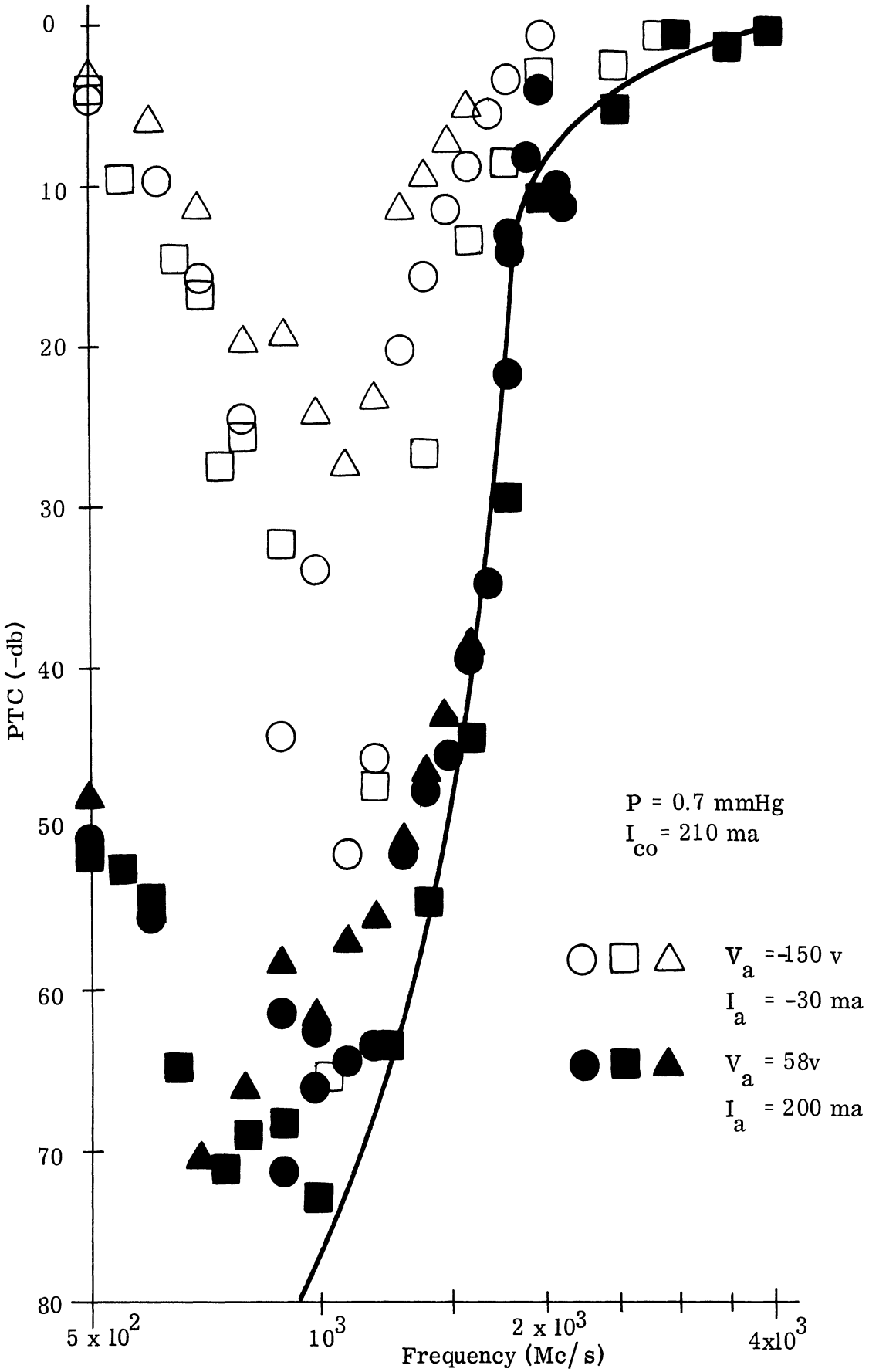

FIG. 2.8: POWER TRANSMISSION COEFFICIENT VS FREQUENCY IN HELIUM DISCHARGE. SOLID LINE IS THEORETICAL CURVE FOR f_p = 1800 Mc AND ν_m = 145 Mc.

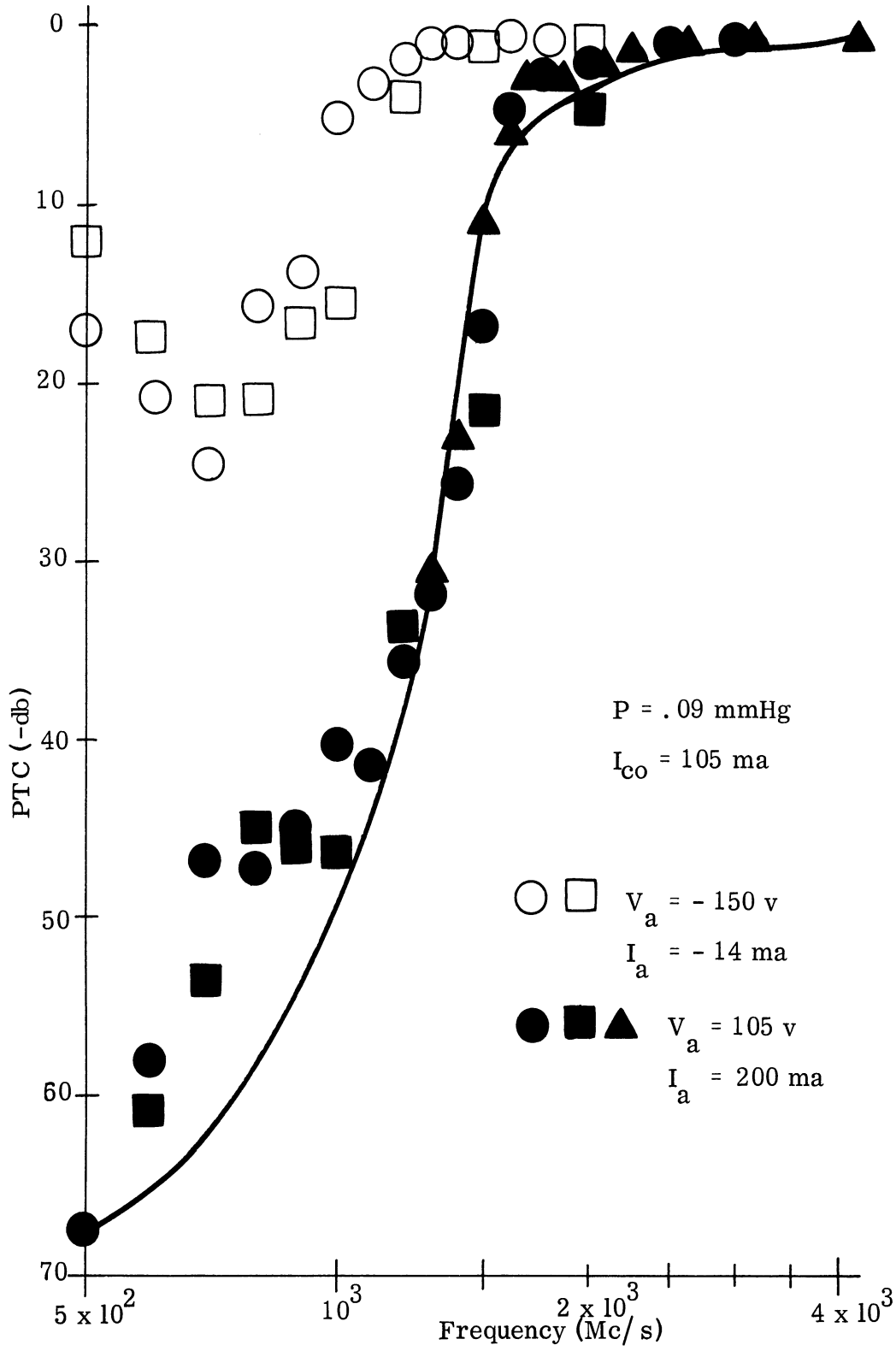

FIG. 2.9: POWER TRANSMISSION COEFFICIENT VS FREQUENCY IN NITROGEN DISCHARGE. SOLID LINE IS THEORETICAL CURVE FOR f_p = 1400 Mc AND ν_m = 150 Mc.

for a sheath of electrons in the cage section close to the grid, with a second lower density region surrounding the anode has been made. The indications are that the -150 volt data may possibly be accounted for theoretically in this manner. A radial dependence of f_p might also account for the behavior of the argon and helium data between 500 and 700 Mc in Case 2. This is being investigated further. It is felt that the experimental data for Case 2 is described well enough by equation (2-3) and that the Lorentzian model is a reasonable one.

Some of the discrepancy between theory and experiment may perhaps be accounted for by errors in the experimental points. A discussion of the possible sources of error in the measurements discussed above is appropriate here. Some of the error sources in the experiment are variation in : 1) gas pressure, 2) cathode discharge current, 3) anode current, 4) probing radio frequency, 5) gas purity and 6) the detection system.

(1, 2, 3) The most serious sources of variations in the measured results are those pertaining to the discharge conditions. Among the pressure, cathode current and anode current, the cathode current was most difficult to maintain at the desired value. For some cases an excursion of 10 per cent in cathode current may have occurred during the course of an experimental run. It required some change in the anode voltage to keep the anode current constant, thus varying the plasma in the grid-anode region. For frequencies sufficiently below the plasma frequency $|\tau^2|$

is essentially an exponential function with a negative real exponent. The negative exponent is determined by the plasma properties. A small change in these properties may produce a large change in the power transmission. Below 1000 Mc a 7 db spread in the data points was common due to this cause when the plasma frequency was 1400 Mc or more. The spread in the data points gradually decreases as the probing frequency is increased above the plasma frequency, as can be judged from Figures 2.7 - 2.9. The pressure excursions did not exceed 10 per cent. A 10 per cent change in gas pressure for a fixed anode and cathode current produced a variation in $|\tau^2|$ of 5 db for argon and 0.5 db for helium and nitrogen. The spread in data points due to gas pressure changes was not severe.

(4) The probing radio frequency was set using the generator dial. The smallest division on the dial was 20 Mc. It is felt that there were no problems in returning to the same frequency within this error. The data spread due to this cause should be minimal. A calibration of the generator frequency dial with a coaxial wave meter indicated an absolute dial accuracy of about 1/2 per cent, while the specifications for the generator list an accuracy of $\pm$ 1 per cent. In the vicinity of the plasma frequency, a 1 per cent error in the probing frequency could be responsible for an error in $|\tau^2|$ on the order of $\pm$ 2 db, for a small collision frequency type plasma.

(5) The purity of the gases used in this experiment was greater than 99.99 per cent, as supplied. Taking into account the measured net pumping rate of the system and the measured leak rate, the minimum gas purities are estimated to be 99.5 per cent at 1 mm Hg and 96.5 per cent at 0.1 mm Hg. The primary contaminants in the system would be nitrogen, oxygen and water vapor which may dissociate into hydrogen and oxygen. Since the collision probabilities of all these gases are, in the electron energy ranges encountered in this experiment, on the same order of magnitude, the effect of the contamination on the measurements of the collision frequency is estimated to be less than 10 per cent. The nitrogen measurements should be least affected, the argon data most, since most argon data was taken in the 0.1 mm Hg range. Since nitrogen, the major impurity, has an ionization potential substantially lower than helium, the plasma frequency in helium might be affected by the presence of nitrogen.

(6) The detection systems used to measure the transmitted power are estimated to have a maximum error of $\pm$ 2 per cent of the db reading, or 0.2 db which ever is greater. The most probable overall error is certainly less than the sum of the absolute instrument calibration errors and the excursions caused by various changes in the discharge. The effect of this error on the analysis of the data is discussed below.

A common method for determining the plasma and collision frequencies from the interaction of electromagnetic waves with a plasma is to measure the

attenuation and phase shift of the transmitted signal at a single frequency, i.e. the complex transmission coefficient. Then separating real and imaginary parts in equation (2-3) one obtains two real independent equations with f_p and ν_m as the unknowns.

As an alternative method to that above for determination of the plasma parameters f_p and ν_m, the amplitude of the power transmission coefficient alone could be measured at two different frequencies. Then putting the experimental values for $|\tau^2|$ into equation (2-3) two independent equations in two unknowns, f_p and ν_m, are obtained. Since these equations involve rather complicated transcendental functions, the solution is best carried out graphically.

If families of $|\tau^2|$ vs frequency curves, with f_p and ν_m as parameters are calculated from equation (2-3), then from the measured $|\tau^2|$ at the single frequency one obtains from these families of curves a discrete set of f_p and ν_m which give the same $|\tau^2|$ as the measured one. For $|\tau^2|$ measured at a second frequency another discrete set of f_p, ν_m are obtained. Each set gives a curve when plotted on the f_p-ν_m plane. Their intersection produces a solution for equation (2-3). Additional $|\tau^2|$ values at different frequencies should produce sets of f_p, ν_m such that all curves have a common intersection for consistent data. A sample graph utilizing this method for three different frequencies is shown in Figure 2.10. As a matter of fact, this is the method used to find f_p and ν_m for the curves of Figures 2.7 - 2.9.

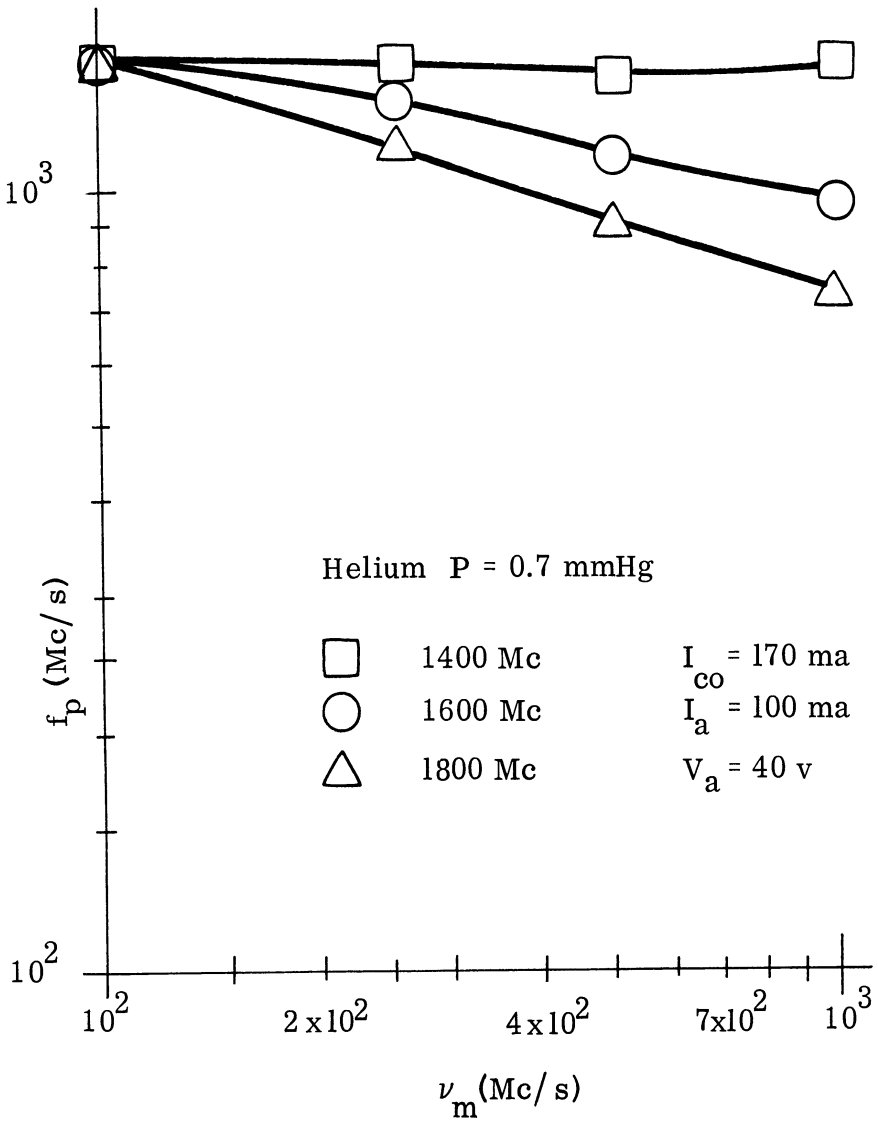

FIG. 2.10: SAMPLE f_p-ν_n PLOT TO DETERMINE PLASMA FREQUENCY AND MOMENTUM TRANSFER COLLISION FREQUENCY FROM RF DATA

Only two measurements need to be taken to find f_p and ν_m. For purposes of checking the consistency of the data as well as reducing the effect of measurement errors, a third frequency can be used. The frequencies used should fall in a portion of the frequency range where the agreement between theory and experiment is good and the experimental data are reasonably accurate. Judging from the curves of Figures 2.7 - 2.9, this would indicate that $|\tau^2|$ less than -40 db should not be used. Because $|\tau^2|$ for frequencies above f_p is most sensitive to ν_m, one of the frequencies used should be greater than f_p.

For f_p between 1000-2000 Mc and $f_p > \nu_m$, a change of 100 Mc in the plasma frequency produces a change in the calculated value of $|\tau^2|$ of about 10 db, when the probing frequency is in the vicinity of the plasma frequency. This is on the same order of magnitude as the maximum uncertainty in the measurements in this region. We conclude that f_p may be obtained accurate to at least within 10 per cent by the method described above, for the plasma length and range of plasma frequencies encountered in this experiment. When ν_m is on the order of 0.1 f_p or less, the same order of accuracy cannot be maintained for the ν_m values. We feel that the uncertainty in ν_m may be a factor of 2 or so.

2.2.1.4 Probe Measurements

The Langmuir probe technique provides another method for determining the plasma and collision frequencies in the discharge, independent of the microwave

measurements. Since the original work of Mott-Smith and Langmuir (Ref. 2.3), probes have been used extensively in plasma research. The technique involves measurement of the probe current as a function of probe voltage. When the probe voltage relative to one of the discharge elements is plotted against the logarithm of the current drawn by the probe, the slope of the resulting curve taken at the appropriate point produces the electron temperature according to

$$T_e = 5080 \frac{\Delta V}{\Delta \log I_e} \qquad (2\text{-}5)$$

where I_e is the electron current and ΔV the change in probe voltage required to produce a change $\Delta \log I_e$. The break current, I_b, where the $\log I_e$-V curve becomes nonlinear, may be used to calculate the electron concentration for a cylindrical probe, according to

$$n_e = 4.029 \times 10^{10} \frac{I_b}{A\sqrt{T_e}} \quad . \qquad (2\text{-}6)$$

In this formula A is the probe area in cm^2, I_b is in ma, and n_e the electron density in electrons/cm^3. The precise point where the break current should be taken is not clearly established. It is usually taken either at the point where the curve becomes nonlinear, or from the intersection of tangent lines drawn to the linear part of the curve and the portion following the break point. This distinction is not important in the case of a plane probe where the break point is quite clearly defined,

but for the cylindrical probe such as was used in this experiment, this is not the case. The tangent method was used in our measurements.

The chamber was provided with a plexiglass end-cover for the probe experiments. A tungsten probe of 0.008 inch diameter with an area of 0.0329 cm^2 was inserted between the grid and anode, about 0.27 cm from the anode and at the midpoint along the length of the cage section. (The probe produced no appreciable effect on the VSWR of the line.) The probe current was sampled by a 1000 ohm resistor, whose voltage drop was fed into a logarithmic converter. (See Fig. 2.6). This output was then fed into the x input of an x-y recorder, while the probe voltage (less the bias voltage) was fed into the y input of the recorder. An example of the probe current curve obtained is shown in Figure 2.11. The no-discharge current is due to the finite input impedance of the x-y recorder. The probe data consistently indicated a Maxwellian velocity distribution for the electrons. Some of the curves obtained exhibited a break in the electron current plot for a low current value indicating the possibility of a second electron distribution of a lower density and higher temperature.

A series of simultaneous probe and RF measurements was carried out for various discharge conditions. The results of these measurements are presented and analyzed in the following section.

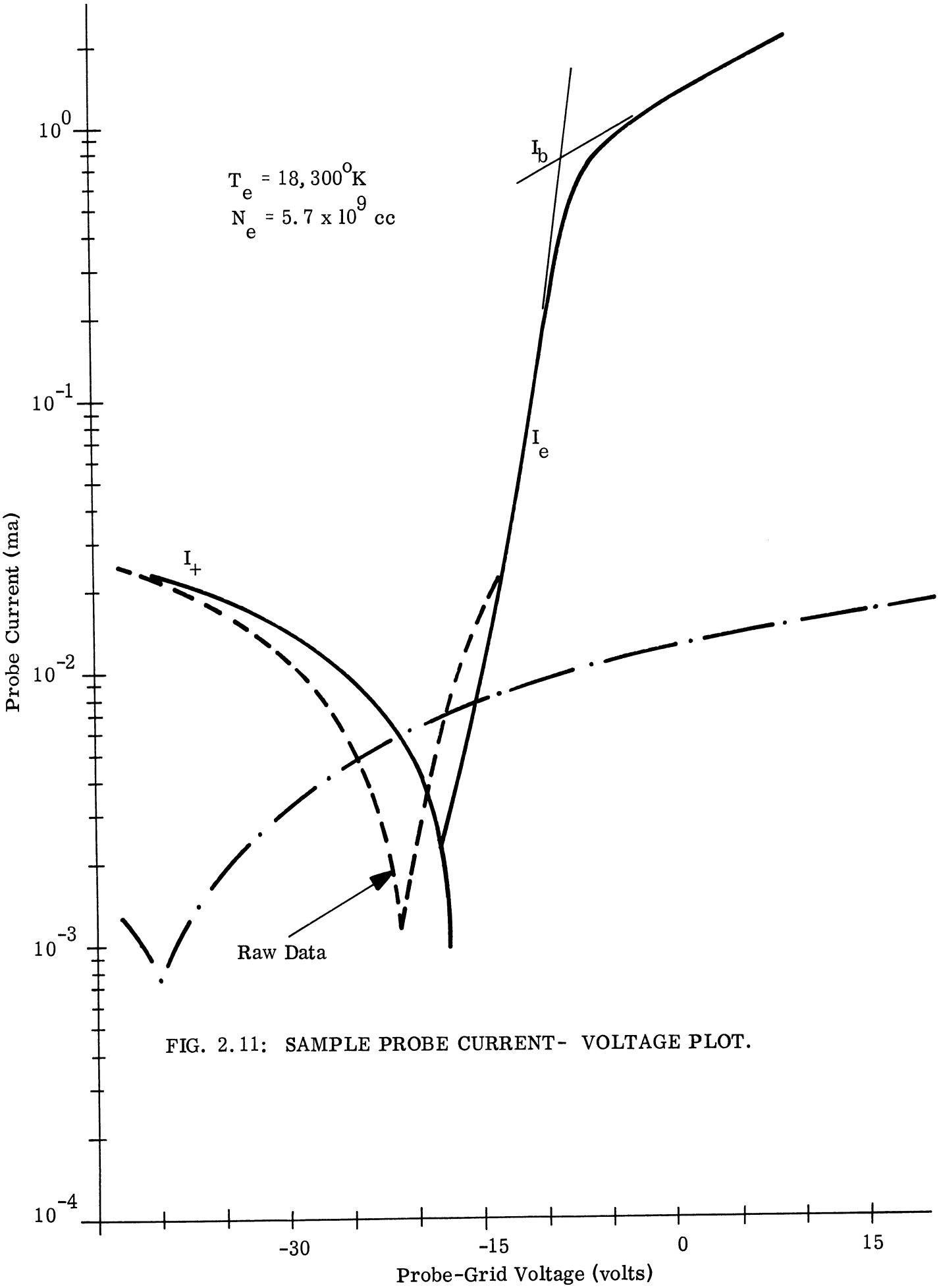

FIG. 2.11: SAMPLE PROBE CURRENT- VOLTAGE PLOT.

2.2.2 The Results

Table 2-I summarizes the results of the simultaneous RF and probe measurements made on the discharge. Columns 1-4 specify the discharge conditions: the pressure, the cathode current drawn by the discharge with the anode circuit open, the anode current and the anode-grid voltage. Columns 5 and 6 give the plasma frequency, f_{pr}, and collision frequency, ν_m, from the RF measurements. The plasma frequency, f_{pp}, and the electron velocity from the probe measurements are listed in Columns 7 and 8. Column 9 gives $P_m(\bar{v})$, the momentum transfer collision probability, calculated as discussed below, and 10 contains values for $P_c(\bar{v})$, the electron collision probability taken at the average electron velocity, from Brown (Ref. 2.4).

The momentum transfer collision frequency for electrons in a gas may be calculated from

$$\nu_m = p_o \int_0^\infty P_m(v)\, v\, F(v)\, dv, \qquad (2\text{-}7)$$

where $p_o = \frac{273}{T} p$, with T the gas temperature in ^oK, p the gas pressure in mm Hg, $P_m(v)$ the momentum transfer collision probability at electron velocity v, F(v) the distribution function for the electron velocities and v is the electron velocity. In the calculations which are discussed below, the temperature of the gas has been taken to be about twice the room temperature, 47^oC or 320^oK.

Discharge Parameters				From RF Data		From Probe Data		$P_m(\bar{v})$	$P_c(\bar{v})$
P	I_{co}	I_a	V_a	f_{pr}	ν_m	f_{pp}	$\sqrt{(3/2)\kappa T_e}$	$(\text{mmHg cm})^{-1}$	$(\text{mmHg cm})^{-1}$
mmHg	ma	ma	volts	Gc	Gc	Gc			
1.8	315	OC	-22	0.66	0.26	0.32	1.31	2.4	20
1.12	210	OC	-35	1.45	0.20	0.78	1.41	2.7	20
1.12	200	200	70	1.55	0.20	0.76	1.54	2.5	20
0.7	170	OC	-36	1.50	0.10	0.88	1.38	2.2	20
0.7	170	100	40	1.55	0.12	1.03	1.19	3.2	19
0.7	200	200	58	1.66	0.16	0.95	1.15	4.3	19
0.38	105	OC	-40	0.92	0.05	0.77	1.15	2.4	19
0.38	105	100	28	1.16	0.09	0.78	1.42	3.6	20
TABLE 2-Ib ARGON									
2.15	440	OC	-13	0.24	1.60	0.27	1.84	8.8	14
2.15	440	400	15	0.75	1.40	0.63	1.73	8.1	14
0.93	325	OC	-15	0.25	0.40	0.26	1.84	5.1	14
0.93	325	300	20	0.65	0.70	0.83	1.51	11.0	11
0.30	200	200	20	0.60	0.10	0.24	1.73	4.0	14
0.13	210	OC	-22	1.05	0.05	1.01	0.98	8.5	4
TABLE 2-Ic NITROGEN									
0.19	210	OC	-14	1.35	0.20	0.96	0.89	26.0	34
0.19	210	200	30	1.30	0.25	0.93	0.87	33.0	33
0.09	105	OC	-10	0.91	0.10	0.71	1.12	22.0	35
0.09	210	200	30	0.60	0.20	0.47	1.98	24.0*	45

p = discharge pressure, mm Hg.
I_a = anode current
f_{pr} = plasma frequency from RF data
f_{pp} = plasma frequency from probe data
$\bar{v}$ = average electron velocity
$P_c(\bar{v})$ = total collision probability from Ref. 2.4.
I_{co} = cathode current with anode circuit open
V_a = anode grid voltage
ν_m = momentum transfer collision frequency from RF data
$P_m(\bar{v})$ = momentum transfer collision probability from RF and probe data.

TABLE 2-I: PLASMA FREQUENCY AND ELECTRON COLLISION PROBABILITY FROM RF AND LANGMUIR PROBE MEASUREMENTS

In the subsequent analysis we are assuming that the electrons have a Maxwellian velocity distribution. In the case when $P_m(v)$ has a rather weak dependence on v, we may approximate equation (2-7) by

$$\nu_m \approx p_o P_m(\bar{v})\, \bar{v}\,, \tag{2-8}$$

where the average velocity

$$\bar{v} = \int_0^\infty v\, F(v)\, dv. \tag{2-9}$$

We may infer the range of validity of this approximation from the following considerations. For a number of gases curves of the electron collision probability, $P_c(v)$, have been obtained by the electron beam method. They are summarized by Brown (Ref. 2.4). The only difference between $P_c(v)$ and $P_m(v)$ is the presence of the $(1-\cos\theta)$ factor for the latter in the integrals defining these quantities in terms of the differential scattering cross section. The scattering angle θ is measured from the forward scattering direction. For isotropic scattering $P_c(v) = P_m(v)$ as well as when the differential scattering cross section is symmetric with respect to $\theta = 90^o$. Calculations based on measured differential scattering cross sections indicate that for most gases $P_m(v)$ agrees with $P_c(v)$ to within $\pm$ 10 per cent for low energy electron scattering. Therefore, we may use the $P_c(v)$ curves to make a judgement on the approximations contained in equation (2-8). Helium does not have a resonance in the region of interest. The approximation should be a reasonable

one for helium. Argon has a resonance in $P_c(v)$ from 1 to 6 $\sqrt{eV}$. Our probe measurements indicate that the RMS average electron velocities in the argon discharge are less than 1.8 $\sqrt{eV}$. Thus, some of the measured values are on the upward slope of the $P_c(v)$ resonance region. The approximation in equation (2.8) is not as good as for helium, but within the range of the probable measurement error. Molecular nitrogen has a resonance in scattering from 1 to 2 $\sqrt{eV}$; a rather sharp peak. The values of $P_m(\bar{v})$ where equation (2.8) is not a reasonable approximation is indicated by an asterisk.

Before commenting on the results summarized in Table 2-I, some general comments concerning the nature of the probe measurements should be made. (1) The probe measures a microscopic electron density in the sense that it is determined in the immediate vicinity of the probe. The RF data give an average measurement. A radial variation in the electron density could tend to make f_{pr} and f_{pp} differ in value. (2) The probe is assumed to have only a small influence on the plasma. However, for many of the measurements, the probe current per unit length was on the order of 25 per cent of the cathode current/unit length. An analysis of the agreement between f_{pr} and f_{pp} in terms of the ratio of probe current/unit length to discharge current/unit length shows that the results obtained with the smaller current ratios do give better agreement.

The plasma frequency from the probe measurements for helium is consistently lower than the plasma frequency from the RF measurements by 16 to 50

per cent. Also, the $P_m(\bar{\nu})$ values are much lower than would be expected from the $P_c(\bar{\nu})$ values. This is even more unusual because the most probable helium contaminants have higher cross sections than helium. Other microwave measurements of P_m are in substantial agreement with those obtained by the electron beam methods.

The f_{pp} for argon varies from 4 to 18 per cent with respect to f_{pr} values, with the exception of one case where it is more. The variation of f_{pp} is above as well as below the f_{pr} values. The $P_m(\bar{\nu})$ values are fairly close to $P_c(\bar{\nu})$ values.

The agreement between the plasma frequencies for molecular nitrogen by the two methods is from 22 to 29 per cent. The $P_m(\bar{\nu})$ values agree reasonably well, except for one case where $P_c(\bar{\nu})$ is near a sharp resonance. Preliminary measurements by other microwave methods are approximately in agreement with these. (Ref. 2.6).

2.2.3 Conclusions

It may be stated that for nitrogen and argon the RF measurements reproduce reasonably well the electron neutral molecule collision probabilities previously found by electron beam methods. There is a consistent and significant unexplained disagreement for helium between our results and the values now accepted. Not only more experimental data, but also some further improvements in the gas purity (as well as modifications in our apparatus) are necessary before one may make unqualified statements on this disagreement.

It is also worth mentioning that the Lorentzian plasma model has been found not to give a very good agreement with the experimental results for frequencies less than half the plasma frequency.

Measurements of the power transmission coefficient at two different microwave frequencies has been advanced and successfully applied as an alternative method of plasma diagnostics. Under the circumstances, the agreement between microwave and Langmuir probe measurements of the plasma frequency is reasonable. It is felt that an improvement may be made by using a smaller diameter probe, and by taking into account a possible radial variation in electron density.

2.3 RF Modulation by a Coaxial Glow Discharge.

This section contains a discussion of some experiments carried out with the coaxial plasma chamber described in Section 2.1. In these experiments, the RF transmitted power is measured, as the discharge anode current is varied in some manner. The experiments may be put into two categories: (1) static measurements in which the discharge conditions are slowly varied to determine the equilibrium plasma RF transmission characteristics, and (2) dynamic measurements where a time-varying anode-grid voltage is used.

A new grid structure consisting of seven 0.125 inch diameter rods on a 1.750 inch diameter, with an open section 10 inches in length was used in the plasma chamber. The impedance of this grid structure has a calculated value of about 97 ohms. The outside conductor of the line tapers from 0.680 inch diameter to 1.750

inch diameter in a distance of 2 inches. The center conductor (or anode) was left unchanged.

2.3.1 Static Measurements

Figure 2.12 shows the circuit arrangement used for the static and dynamic measurements. For the dynamic measurements, the desired wave form is fed into the modulator amplifier, and its output is supplied to the anode-grid circuit. The modulator B^+ supply voltage is varied to change the anode-grid voltage for the static measurements.

The power transmission coefficient (PTC) is plotted as a function of the anode current and anode-grid voltage in Figures 2.13 and 2.14 for various pressures. I_{co} is the cathode current with the anode circuit open. This value is reported because cathode current depends to some extent also on the anode current. It is seen in the curve of Figure 2.13, as the pressure is decreased from 0.32 to 0.22 mm Hg with I_{co} held constant, that the curve changes from one with a variation in PTC of less than 5 db as a function of anode current, to a curve with a variation of 37 db. However, as the pressure is further decreased to 0.12 mm Hg, the loss in transmitted power at zero anode current (this will be referred to as the insertion loss) increases markedly with an accompanying decrease in the variation of the PTC as a function of anode current. As this same behavior is exhibited at other pressure and I_{co} combinations, one might conclude that there is a relationship between the

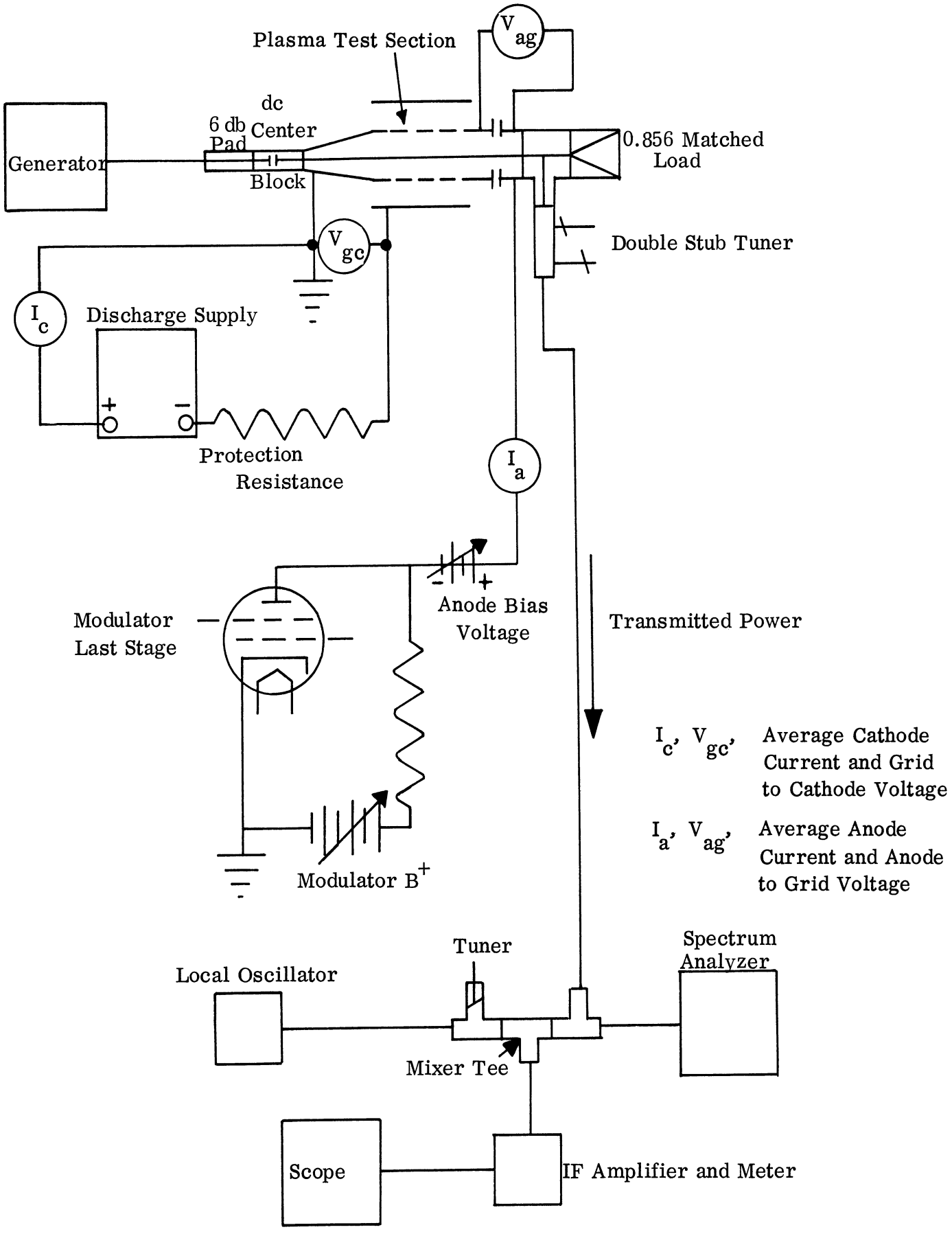

FIG. 2.12: CIRCUIT ARRANGEMENT

pressure and I_{co} that will lead to a maximum power transmission variation for a given anode current range, together with a minimum insertion loss. A rather similar behavior is observed in Figure 14 under like circumstances with the anode to grid voltage being the independent variable. It is noticed that these attenuation graphs exhibit a nearly linear behavior for a combination of pressures and cathode currents.

It is worthwhile noting that the cathode currents used here are small compared with those used previously to obtain PTC vs. frequency data. At 0.1 mm Hg with N_2 gas for example, an I_{co} of 105 ma was used previously, and an insertion loss on the order of 50 db was observed.

2.3.2 Dynamic Measurements

In the dynamic experiments, the anode-grid voltage is varied as a function of time, the input to the modulation amplifier being either a square wave or a complex wave form such as music or speech. In a resistance load and with a reasonable drive the modulation amplifier is a linear device. The results of these tests are discussed below.

(1) Square-wave Testing. An HP 211A square wave generator is used to drive the modulator amplifier which was designed to deliver 100 volts peak to peak across a 100 Ω load. A 100 Ω resistance was connected in parallel with the anode-grid circuit to act as a ballast and improve the voltage wave form. A typical anode-grid voltage rise time is less than 1 microsecond. The dynamic modulation

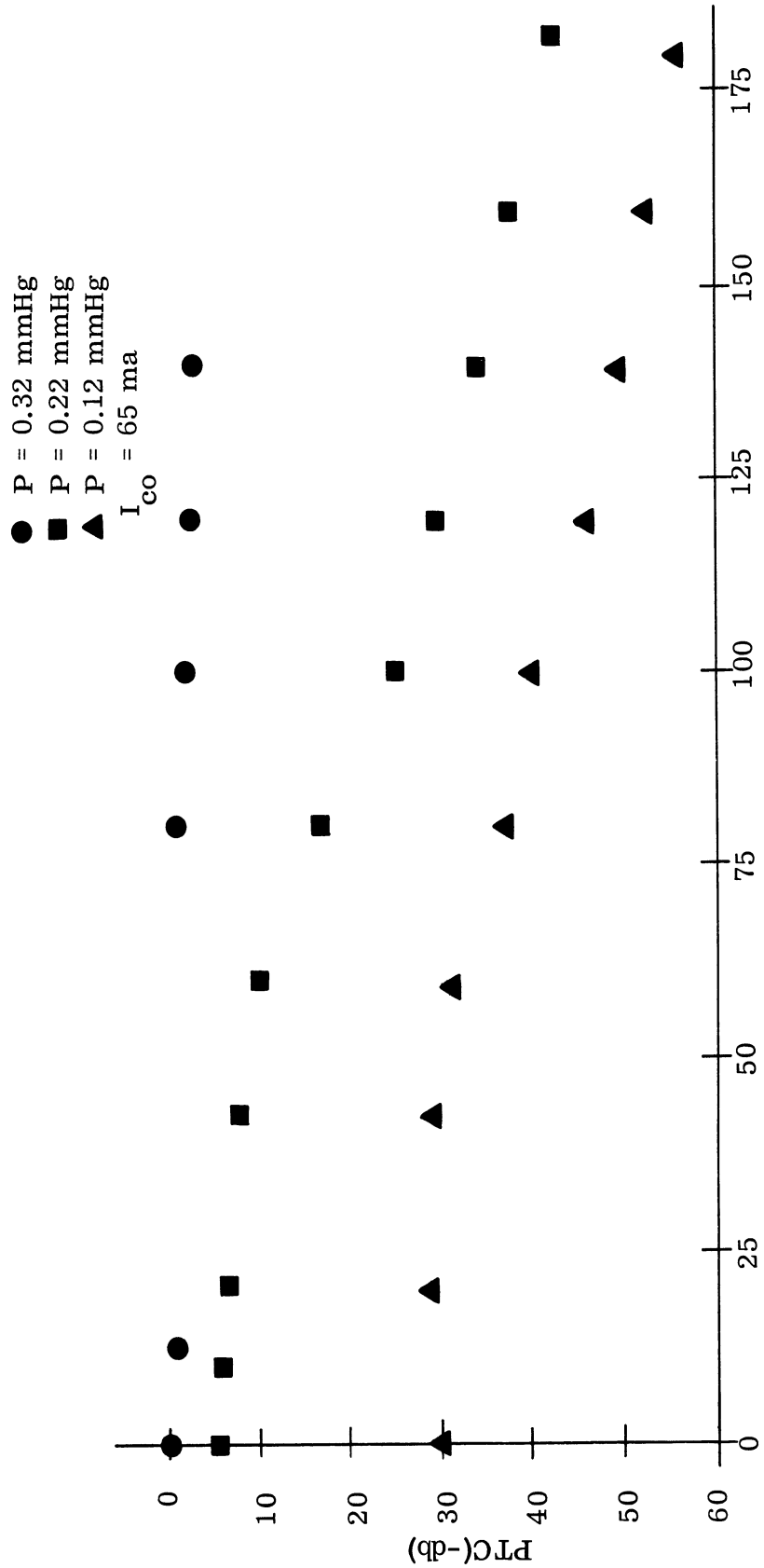

FIG. 2.13: PTC AS A FUNCTION OF ANODE CURRENT, ANODE-GRID VOLTAGE, AND GAS PRESSURE IN NITROGEN f = 1000 Mc

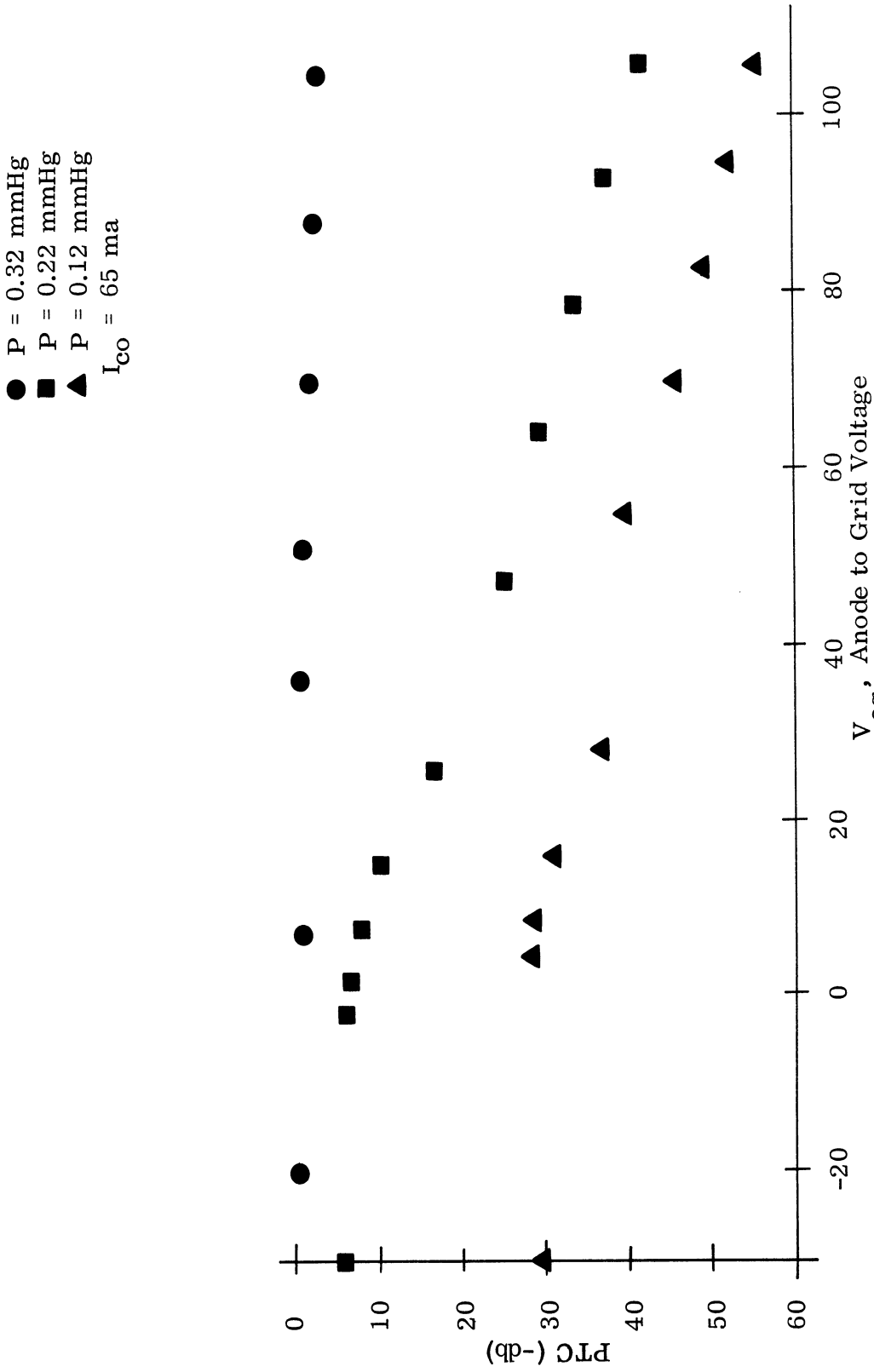

FIG. 2.14: PTC AS A FUNCTION OF ANODE CURRENT, ANODE-GRID VOLTAGE, AND GAS PRESSURE IN NITROGEN. f = 1000 Mc .

measurements were conducted primarily with nitrogen. Argon and helium were used less extensively. Measurements were performed at RF frequencies of 925 and 1000 Mc and a square wave modulation frequency of 500 cps. The parameters measured are

(a) $\Delta T(\frac{1}{2} I_a)$. Anode current rise time, defined as the time required for the anode current to rise to half its maximum value.

(b) $\Delta T(\frac{1}{2}|\tau|)$. The attenuation rise time defined as the time required for the transmitted voltage to decrease to half its maximum value.

(c) $\left|\frac{\tau_{min}}{\tau_o}\right|^2$. The minimum attenuation relative to the no plasma case.

(d) $\left|\frac{\tau_{max}}{\tau_{min}}\right|^2$. The maximum to minimum attenuation due to plasma modulation.

(e) The time required for the anode current and transmission loss to decrease to half the maximum value (decay time).

Table 2-II contains the results of the rise time measurements as a function of the gas pressure, while keeping the peak-to-peak anode grid voltage, V_{pp}, and the anode bias voltage, V_b, relatively constant. These results indicate that the anode current rise time and the attenuation rise time do not differ greatly from each other, or change appreciably for modest changes in the pressure or with any of the gases used. These values are generally on the order of 10 to 20 microseconds. The decay times for the anode current and the attenuation are on the same order of magnitude.

The maximum change in attenuation is about 20 db, with an insertion loss of up to 4 db. The data was obtained by fixing the gas pressure, while varying the cathode current until the transmitted power was judged to have the best square wave response attainable. The peak-to-peak anode to grid voltage ranged from 80 to 90 volts and the bias ranged from 15 to 20 volts. The data presented are substantially in agreement with expected values from the static measurements of Figures 2.13 and 2.14.

The $\Delta T(\frac{1}{2}|\tau|)$ values do not include the time interval taken up by the oscillation in the leading edge of the transmitted power as shown in the photographs of Figure 2.15. This peculiarity in the wave form was encountered in the lower range of the pressures used and added a maximum of 50 microseconds to the rise time, yielding the values in the $\Delta T'(\frac{1}{2}|\tau|)$ column, which do thus show a pressure dependence.

Rise time measurements were carried out as the peak-to-peak modulation voltage alone was varied. Also, some measurements were done for the case where the anode bias voltage alone is varied. Both experiments were performed using nitrogen gas at a pressure of 0.090 mm Hg. In each case, the cathode current was set at a value producing the best modulation envelope. From the data it was seen that the attenuation rise time increases and the attenuation decreases when either the peak-to-peak anode-grid voltage or the bias voltage are decreased.

DISCHARGE PARAMETERS						RISE TIMES			ATTENUATION	
	P	I_c	V_{gc}	V_{ag}	I_a	$\Delta T(\frac{1}{2} I_a)$	$\Delta T(\frac{1}{2}\lvert\tau\rvert)$	$\Delta T'(\frac{1}{2}\lvert\tau\rvert)$	$\left\lvert\frac{\tau_{min}}{\tau_o}\right\rvert^2$	$\left\lvert\frac{\tau_{max}}{\tau_{min}}\right\rvert^2$
	mm Hg	ma	volts	volts		μ sec	μ sec	μ sec	db	db
NITROGEN	.19	152	300	55	135	10	10	10	3	15
	.14	86	272	58	88	15	20	60	3	16
	.10	55	272	60	58	18	10-15	55	3	14
	.074	34	268	62	35	20	15	65	3	13
	.040	25	298	64	25	20	10-15	35	3	15
	.027	22	345	63	22	18	10	20	1-2	18
	.018	30	400	62	31	18	8	18	1-2	18
HELIUM	.66	28	268	64	29	10	10	10	4	14
	.30	10	288	65	10	20	20	50	1.5	14.5
	.088	15	375	65	15	20	10	20	3	16
	.055	24	452	64	23	16	10	30	3	19

TABLE 2-II: ANODE CURRENT AND ATTENUATION RISE TIMES, INSERTION LOSS, AND MAXIMUM ATTENUATION CHANGE AS THE GAS PRESSURE AND CATHODE CURRENTS ARE VARIED

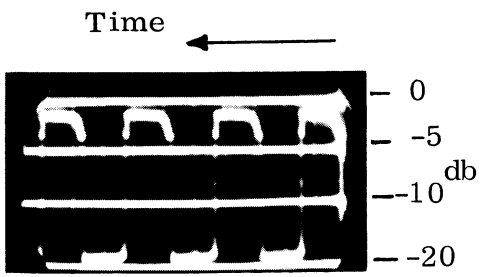

RF MODULATION ENVELOPE

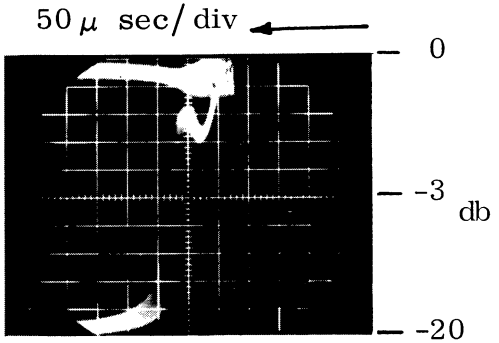

LEADING OF RF MODULATION ENVELOPE

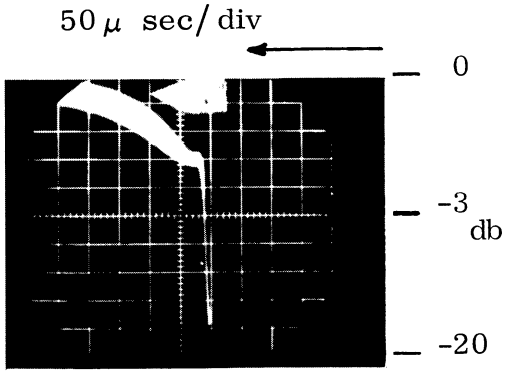

TRAILING EDGE OF RF MODULATION ENVELOPE

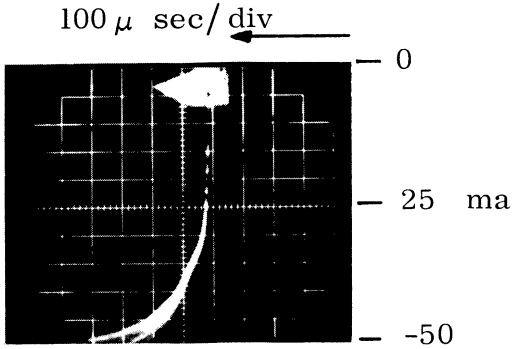

LEADING EDGE OF ANODE CURRENT

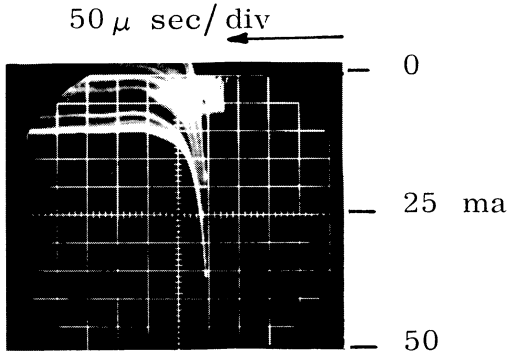

TRAILING EDGE OF ANODE CURRENT

FIG. 2.15: THE RF MODULATION ENVELOPE OF 500 CPS ON 1000 Mc. RF. NITROGEN GAS DISCHARGE AT 0.04 mm Hg.

A study of the 500 cps square wave modulation envelope on the 1000 Mc RF wave as a function of cathode current and the nitrogen gas pressure is indicated in Figure 2.16. One observes from the synchroscope pictures that the detected wave shape depends rather critically on the proper combination of gas pressure and cathode current. Decreasing or increasing either one severely affects the modulation process. The very first picture shows the optimum wave shape obtainable.

At pressures less than 0.1 mm Hg for argon and nitrogen gas, and 0.2 mm for helium the discharge has the appearance of a very tenuous glow in the cathode-grid region. The grid-anode region has a uniform, brighter glow. For certain discharge conditions in this pressure range, the discharge may be turned on and off by applying and removing the anode modulating voltage.

Frequently, a high frequency oscillation is seen in both the anode current and the transmitted wave forms. This oscillation has a frequency of 100-300 kc, in the pressure range 0.2 mm to 0.5 mm for nitrogen, and appears both when the anode current is at its maximum value and minimum value. The frequency of oscillation seems to increase from 0.2 to 0.5 mm, then decrease again as the pressure is raised and is almost gone at 1.0 mm Hg.

2.3.3 Sound Modulation

In this experiment, a voice or music signal was used as the anode modulating source. The modulated RF wave was mixed with a local oscillator signal to

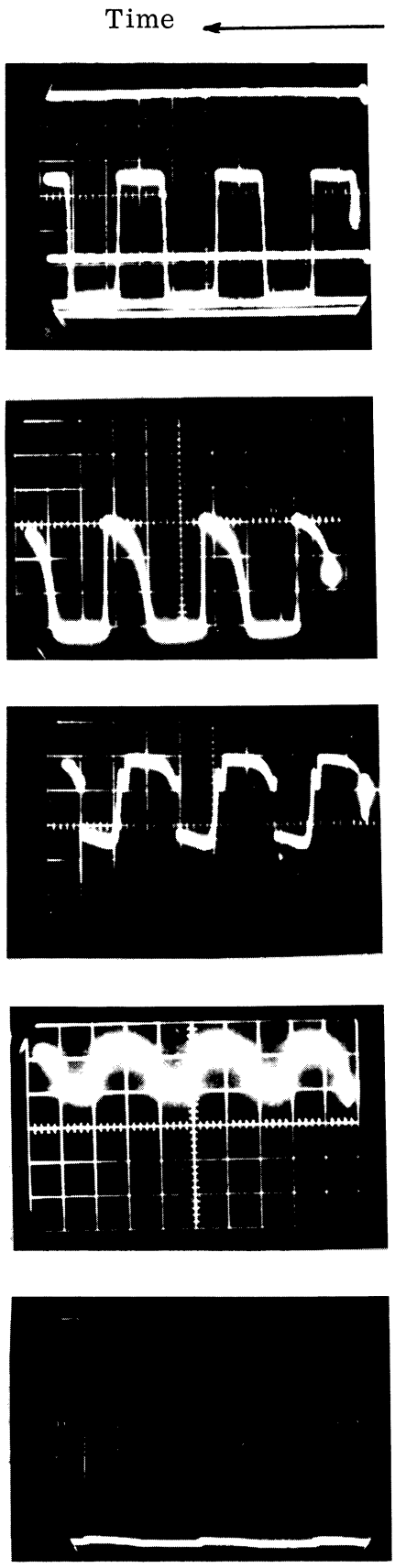

FIG. 16: STUDY OF 500 cps ENVELOP IN 1000 Mc RF WITH NITROGEN DISCHARGE PRESSURE AND CATHODE CURRENT AS VARIABLES.

FIG. 2.16: STUDY OF 500 cps ENVELOPE IN 1000 Mc RF WITH NITROGEN DISCHARGE PRESSURE AND CATHODE CURRENT AS VARIABLES

produce a 30 Mc beat frequency which was fed into a standard communication receiver. The best results were obtained in the pressure range of 0.2 to 0.5 mm Hg using helium gas. The fidelity of the signal was not good, although speech was understandable. Music was quite distorted, with little dynamic range.

2.3.4 Conclusions

The modulation experiments demonstrate that a glow discharge may be effectively used as a variable attenuator or as a moderately fast switch of RF power. When used as a variable attenuator, the discharge has these properties:

(1) Adjustable attenuation from 0 to 80 db at 1000 Mc by varying the anode and cathode currents.

(2) Useful frequency range from about 200 to 1500 Mc; attenuation in frequencies outside this range becomes less than 30 db.

Operating the discharge as a modulator with an anode bias voltage of 15 to 20 volts and a peak-to-peak square wave voltage of 80 to 90 V, the following characteristics are observed:

(1) The insertion loss (loss with anode current at its minimum value) is about 2 or 3 db.

(2) A minimum to maximum transmitted power change of 18 to 20 db can be obtained.

(3) The time required for the transmission voltage to decrease to half its

maximum value is on the order of 20 to 50 microseconds. The decay times for the loss are on the same order of magnitude.

(4) At any pressure there is a limited range of cathode currents which leads to the best square wave response of the transmitted power.

Shorter rise times and peak-to-peak transmission losses greater than 20 db may be obtained by increasing the peak-to-peak modulation voltage. Decreasing the bias voltage reduces the insertion loss.

REFERENCES FOR SECTION II

2.1 G. R. Nicoll and J. Basu, "Comparison of Microwave and Langmuir Probe Measurements on a Gaseous Plasma," J. Electronics and Control, Vol. XII, No. 1, 23-29 (January 1962).

2.2 R. W. P. King, Transmission Line Theory, p. 43, McGraw-Hill Book Co., Inc., New York (1955).

2.3 H. M. Mott-Smith and L. Langmuir, "The Theory of Collectors in Gaseous Discharges," Phys. Rev., 28, 727-763 (October 1926).

2.4 S. C. Brown, Basic Data of Plasma Physics, Ch. I. John Wiley and Sons (1959).

2.5 L. Gould and S. C. Brown, "Microwave Determination of the Probability of Collisions in Gases," Phys. Rev., 95, No. 4, 897 (August 1954).

2.6 A. Phelps, O. T. Fundingsland and S. C. Brown, "Microwave Determination of the Probability of Collisions of Slow Electrons in Gases," Phys. Rev., 84, No. 3, 559 (November 1951).

III

ELECTRON CYCLOTRON RESONANCE ISOLATOR

3.1 Introduction

A uniform static magnetic field $\bar{B}_0 = B_0 \bar{a}_x$ impressed on a plasma gives rise to a cyclotron frequency (or gyroelectric frequency)

$$\bar{\omega}_H = (|e|/m) B_0 \bar{a}_x \qquad (3\text{-}1)$$

where e and m are the electronic charge and mass respectively and $\bar{a}_x$ is a unit vector. If a microwave field of angular frequency ω propagating in this plasma has a circularly polarized electric field in a plane normal to $\bar{a}_x$ then strong absorption will occur if these two conditions are met simultaneously:

(1) $|\bar{\omega}_H| = \omega$,

(2) the direction of rotation of the circularly polarized electric field is the same as $\bar{\omega}_H$.

(f and f_H which appear later are defined by $\omega = 2\pi f$, $\omega_H = 2\pi f_H$.) This is because the electric field is in synchronism with the electrons and will convert electromagnetic energy into mechanical energy, i.e. increase the linear velocity of the electrons rotating about the static magnetic field lines and by collisions with neutrals this energy is converted into thermal energy.

The absorption mechanism of electromagnetic waves discussed above may be used to design a resonance isolator. Consider a square waveguide and the coordinate system as shown in Figure 3.1. Of particular interest is the TM_{11} mode

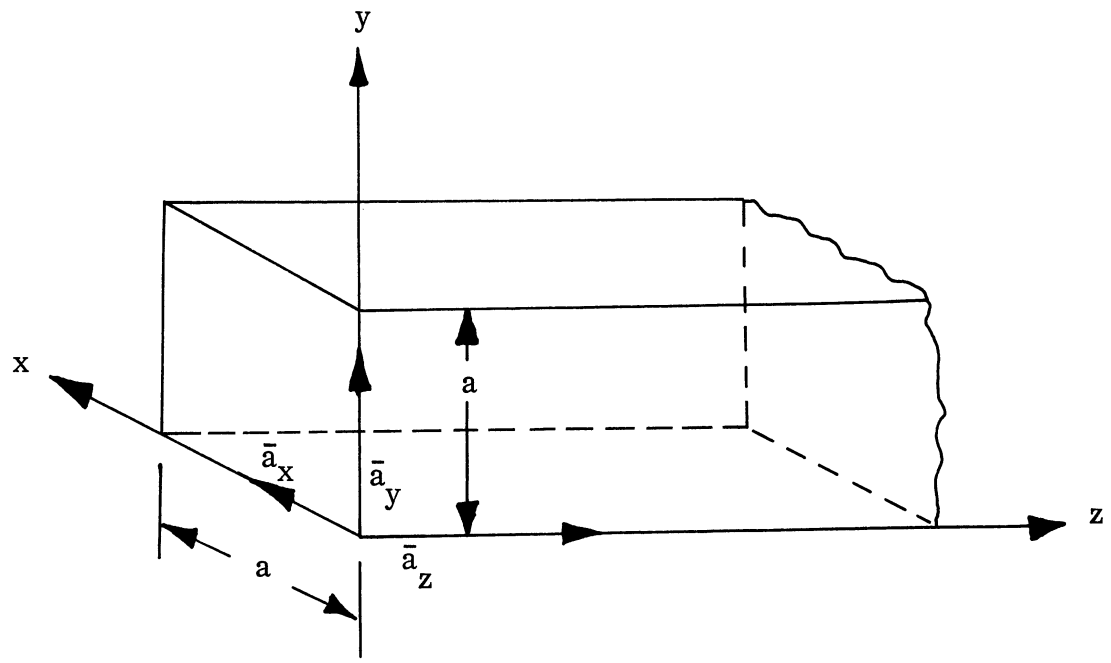

FIGURE 3.1

COORDINATE SYSTEM

which is the lowest propagating TM mode. For propagation in the positive z-direction, with $e^{j\omega t}$ assumed, the fields of this mode are (Ref. 3.1)

$$\bar{E} = A\left[-\frac{j\beta_{11}a}{2\pi}\cos\frac{\pi x}{a}\sin\frac{\pi y}{a}\,\bar{a}_x - \frac{j\beta_{11}a}{2\pi}\sin\frac{\pi x}{a}\cos\frac{\pi y}{a}\,\bar{a}_y + \sin\frac{\pi x}{a}\sin\left(\frac{\pi y}{a}\right)\bar{a}_z\right]e^{-j\beta_{11}z} \tag{3-2}$$

$$\bar{H} = \frac{j\omega\epsilon_o a}{2\pi}A\left[\sin\left(\frac{\pi x}{a}\right)\cos\left(\frac{\pi y}{a}\right)\bar{a}_x - \cos\left(\frac{\pi x}{a}\right)\sin\left(\frac{\pi y}{a}\right)\bar{a}_y\right]e^{-j\beta_{11}z}. \tag{3-3}$$

We notice that the electric field in the y-z plane is elliptically polarized. We denote the amplitude of this field by $E^{(+)}_{y-z}$ and get

$$\bar{E}^{(+)}_{y-z} = A\left[-\frac{j\beta_{11}a}{2\pi}\sin\frac{\pi x}{a}\cos\frac{\pi y}{a}\bar{a}_y + \sin\frac{\pi x}{a}\sin\frac{\pi y}{a}\bar{a}_z\right]. \tag{3-4}$$

We obtain the TM_{11} mode travelling in the negative z-direction by letting $\beta_{11} \rightarrow -\beta_{11}$ in equations (3-2) and (3-3), Denoting the electric field of this mode in the y-z plane by $E^{(-)}_{y-z}$, we have

$$\bar{E}^{(-)}_{y-z} = B\left[\frac{j\beta_{11}a}{2\pi}\sin\frac{\pi x}{a}\cos\frac{\pi y}{a}\bar{a}_y + \sin\frac{\pi x}{a}\sin\frac{\pi y}{a}\bar{a}_z\right]. \tag{3-5}$$

We notice from equation (3-4) that the sense of polarization for $a/2 < y < a$ is opposite to that for $0 \leq y \leq a/2$. The same holds true for the reflected wave, i.e. equation (3-5). Furthermore, $E^{(-)}_{y-z}$ has an opposite sense of polarization to that of $E^{(+)}_{y-z}$. Therefore with a dc magnetic field in the x-axis direction and with a plasma filling a part of either the lower half or the upper half of the waveguide we will get selective absorption depending on the direction of the wave travel. Furthermore, if the plasma slab is placed where the electric field is circularly polarized then absorption will occur only in one direction of wave travel.

3.2 The Experimental Device

Figure 3.2a is a scale cross section drawing of the isolator on the longitudinal axis. Figure 3.2b is a transverse section through the center of the isolator chamber. The figures show the location of the plasma chamber and the mode-suppressors. The TEM to TM_{11} mode transducer consists of a tapered square outside conductor and a tapered circular inside conductor, which is supported at the transition to the coaxial line by a teflon bead.

The magnetic field is applied to the isolator in a direction normal to the plane of the drawing of Figure 3.2a. In the discussion to follow, the magnetic field values given will be those measured at the center of the plasma chamber. The significant variation in the magnetic field over the volume occupied by the plasma chamber was found to be about $\pm$ 15 per cent with respect to the field at the center of the chamber. Repeatability of magnetic field values are within 2 per cent.

Figures 3.3 and 3.4 show the no-plasma isolator insertion loss and the power reflection coefficient in db as a function of frequency, with and without mode suppressors in place. In all the drawings, note that curves shown without data points indicate that the independent variable was changed continuously, and the appropriate parameters continuously recorded by an x-y recorder.

Before we further comment on these curves we should discuss the mode picture in the structure. For the successful operation of the device in a rectangular waveguide we require only the fields of the TM_{11} mode. The cut-off frequency of

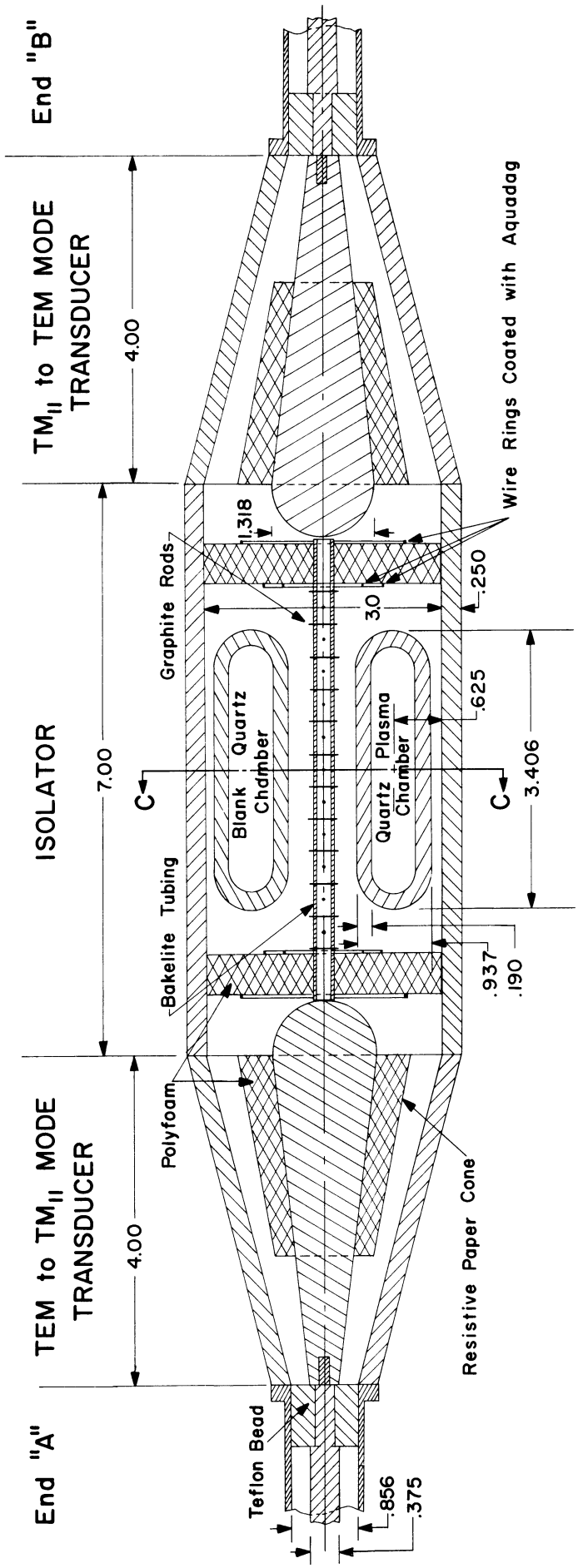

FIG. 3.2a: PLASMA CYCLOTRON RESONANCE ISOLATOR WITH SPURIOUS MODE SUPPRESSORS

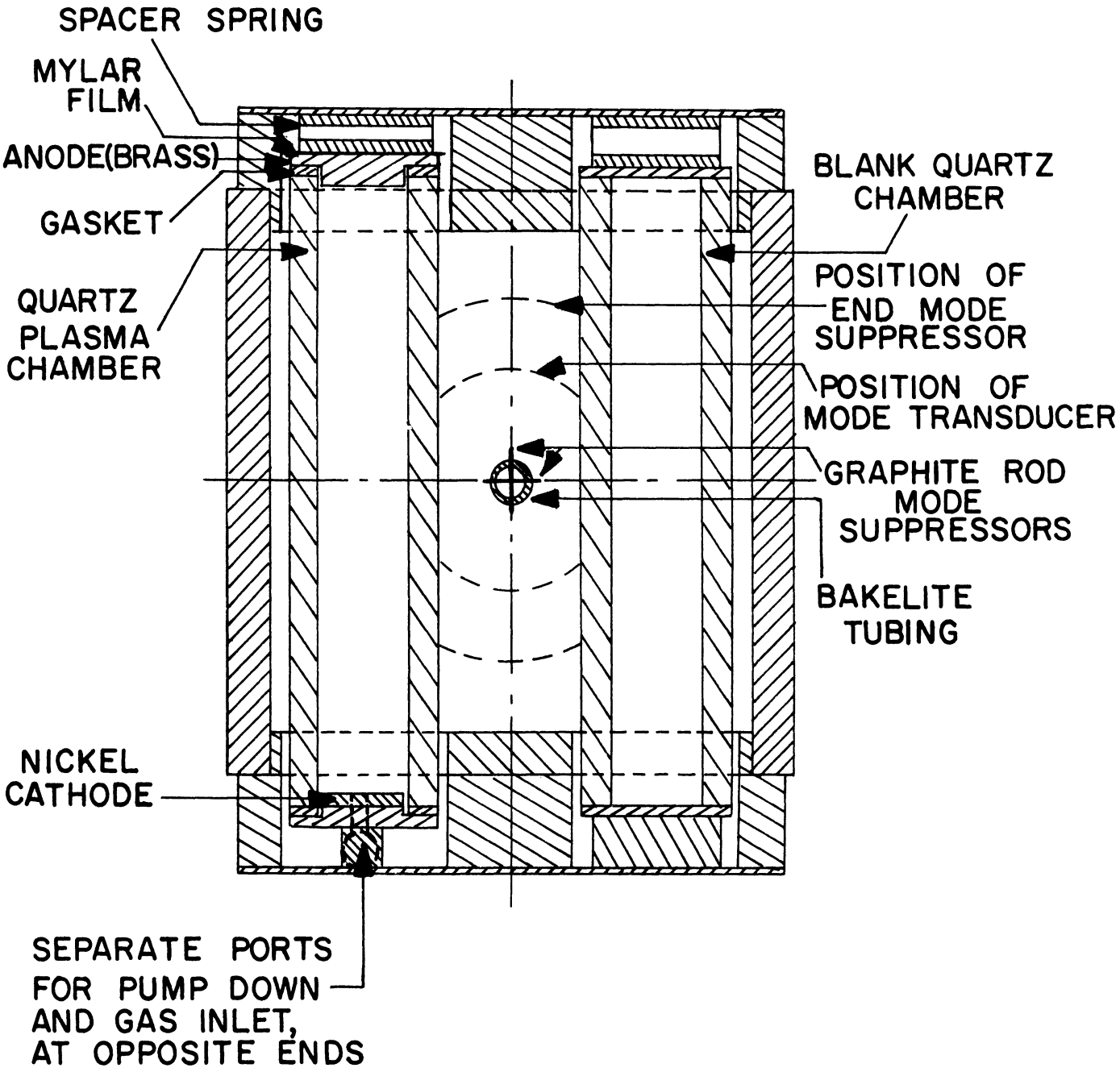

FIG. 3.2b: CROSS SECTION VIEW OF ISOLATOR

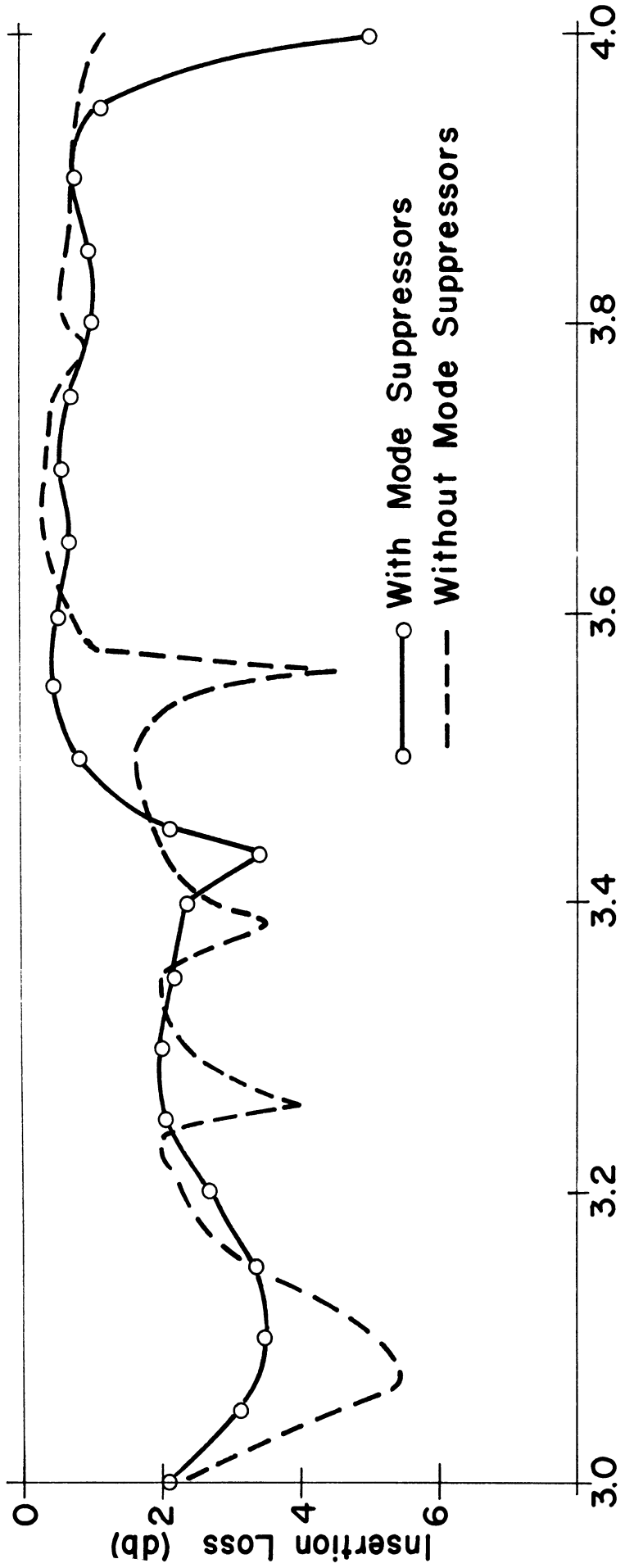

FIG. 3.3: NO-PLASMA INSERTION LOSS WITH AND WITHOUT MODE SUPPRESSORS

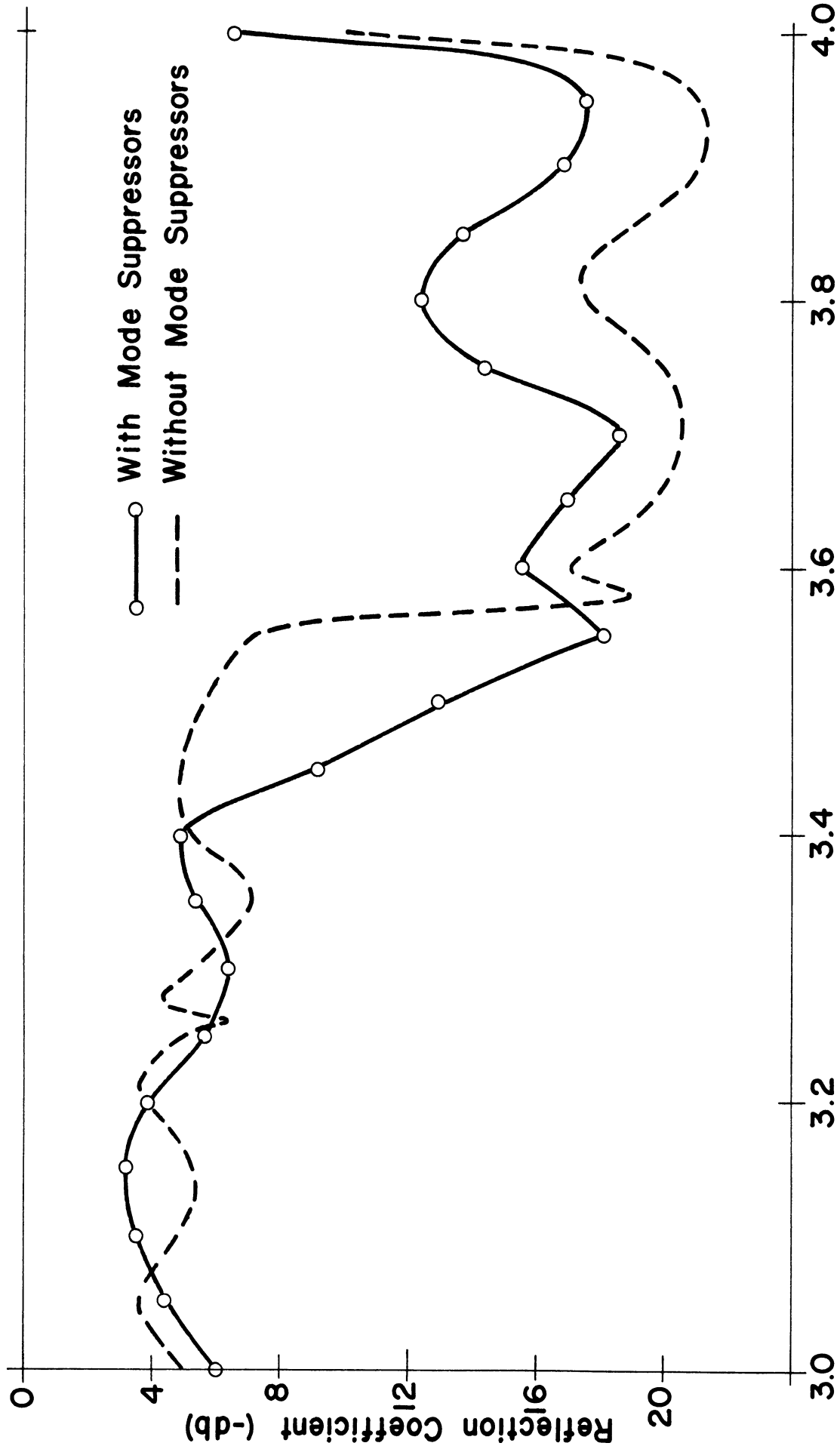

FIG. 3.4: NO-PLASMA POWER REFLECTION COEFFICIENT WITH AND WITHOUT MODE SUPPRESSORS

the TM_{11} mode is 2.78 Gc. The cut-off frequency of the TE_{10} and TE_{01} modes is 1.97 Gc. That of the TE_{11} mode is the same as for the TM_{11} , and of the TE_{20} and TE_{02} it is 3.94 Gc. If we operate the device from 3 to 4 Gc, we have to contend with the fact that TE_{10}, TE_{01} and TE_{11} may exist, and very close to 4 Gc, the TE_{02} or TE_{20} may also start propagating. We observe that the mode transducer joining the co-ax to the rectangular waveguide provides symmetric excitation with respect to the guide axis. The undesirable modes require unsymmetric excitation, and thus they will not be excited by the transducer itself. However, since the TM_{11} mode requires symmetric excitation, it will be induced. The chamber requires a plasma slab in an unsymmetric position. So in order to keep the asymmetry as low as possible, a blank quartz chamber was introduced on the opposite side. However, some asymmetry still remains in the rectangular sections even without plasma and it couples energy out of the desirable mode into the undesirable ones. This energy cannot get out of the isolator section because the fields of these modes do not satisfy the transducer symmetry requirements and the isolator becomes a cavity for such modes. A calculation on the basis of a rectangular cavity shows that resonances may occur at ten frequencies in the interval from 3 to 4 Gc. In addition, considerable degeneracy exists, i.e. a number of modes may have the same frequency of resonance. The frequency difference between some of these resonances is small. Thus they may coalesce to form a single absorption peak. In fact, in Figure 3.3,

we see only five absorption peaks for the case of no mode suppressors. Mode suppressors were added as indicated in Figure 3.2a in the hope that some of these unwanted resonances would either be suppressed outrightly, or that the resonant effect would be reduced appreciably as a result of a lower Q for the respective resonances. The mode suppressors have removed some of the resonance peaks in the insertion loss resulting in generally smoother curves. The reflected power is increased somewhat by the mode suppressors between 3.6 and 4.0 Gc, however, but the VSWR in this range still remains less than 1.5.

Much of the data obtained in this experiment was taken before the mode suppressors were available. Data taken after the addition of the mode suppressors will be indicated.

3.3 Discharge Properties.

The plasma in the magnetic field is a glowing gas and appears to be quite uniform over the volume of the chamber. Argon at a pressure of about 0.15 mm Hg was used in obtaining the data presented here. The voltage required to obtain a given discharge current was found to decrease as the magnetic field was increased. For example, an increase of magnetic field from 0 to 1800 gauss at a 10 ma discharge current resulted in a decrease of the discharge voltage by 12 per cent. The voltage required for a constant discharge current was found to decrease with time after initiation of the discharge until an equilibrium condition was reached. This decrease

was about 30 per cent of the initial voltage. The equilibrium voltage was about 550 volts with 10 ma current.

Solid end plates were put on the isolator section and small loop probes were used to couple weakly into a TE_{011} resonant mode. The cavity Q and shift in resonant frequency were measured with the microwave electric field parallel to the DC magnetic field for various discharge currents and magnetic fields. A determination of the electron density and electron collision frequency could then be made (Ref. 3.2). Figure 3.5 shows the plasma frequency as a function of discharge current for two magnetic field strengths. It is interesting to note that this data is described by $f_p = K\sqrt{i}$. This implies that the electron drift velocity is relatively constant over a wide range of current and magnetic field values. The electron collision frequency determined from the cavity data varied between 1.2 and 0.4 Gc, decreasing with increasing magnetic field.

3.4 Variable Frequency Characteristics of Isolator.

The transmission and reflection characteristics of the isolator were investigated over the frequency interval 3.0 to 4.0 Gc for various discharge currents and magnetic fields. Measurements were taken in both directions, for magnetic fields of 500 gauss to 2000 gauss and discharge currents of 0.5 ma to 20 ma. The maximum value of discharge current that could be used without causing the discharge to become unstable was 20 ma. Some typical examples of the data obtained will now be discussed.

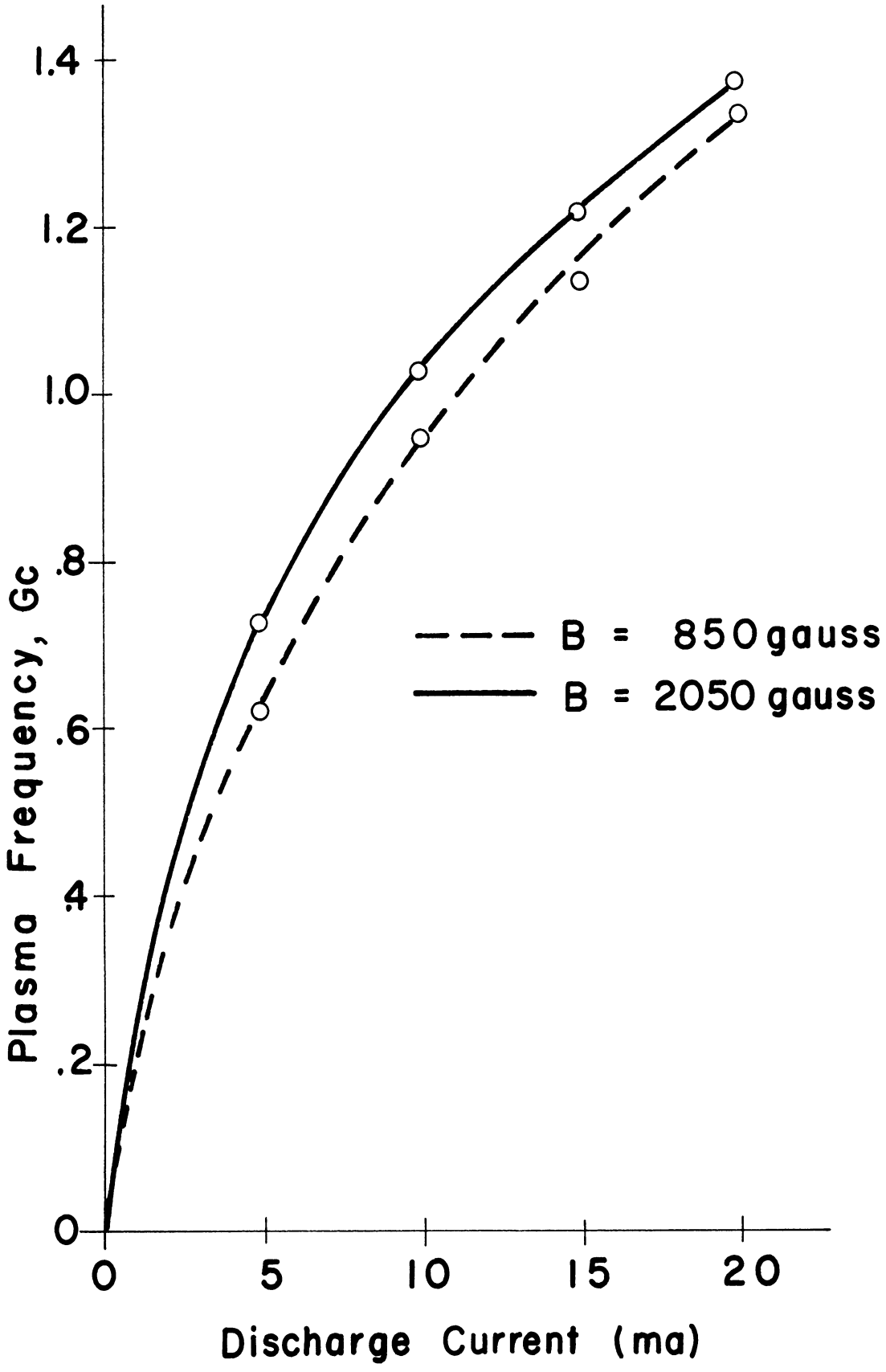

FIG. 3.5: ISOLATOR PLASMA FREQUENCY VS DISCHARGE CURRENT

In Figure 3.6 we show the isolation (Direction A) and insertion loss (Direction B), from 3.5 to 4.0 Gc for discharge currents of 4, 8 and 16 ma. Only the 16 ma curve is included for Direction B since the other data is quite similar. The non-reciprocity of the isolator is immediately evident. What was unexpected, however, was that the isolation is more than 10 db, over an appreciable portion of the 500 Mc band. The isolation at about 3.65 Gc is greater than 30 db (on subsequent graphs, the intersection of the frequency axis by the curve indicates attenuation of more than 30 db). A strong dependence of the isolation upon the plasma frequency is also evident.

Figures 3.7 and 3.8 present isolation and insertion loss curves from 3.0 to 4.0 Gc for a fixed value of discharge current and magnetic fields of 1300, 1440 and 1560 gauss. Again, the transmission is non-reciprocal. The insertion loss is generally less than 4 db while the isolation is greater than 10 db over much of the frequency interval. The large isolation values, some exceeding 20 db, are felt to be associated with resonances. The reasons for this conclusion are that the frequency at which a typical peak occurs does not seem to have any particular relation to the cyclotron frequency f_H, but can be correlated with the no-plasma resonances. Also, changes in f_H do not produce equivalent corresponding shifts in the frequencies of maximum absorption.

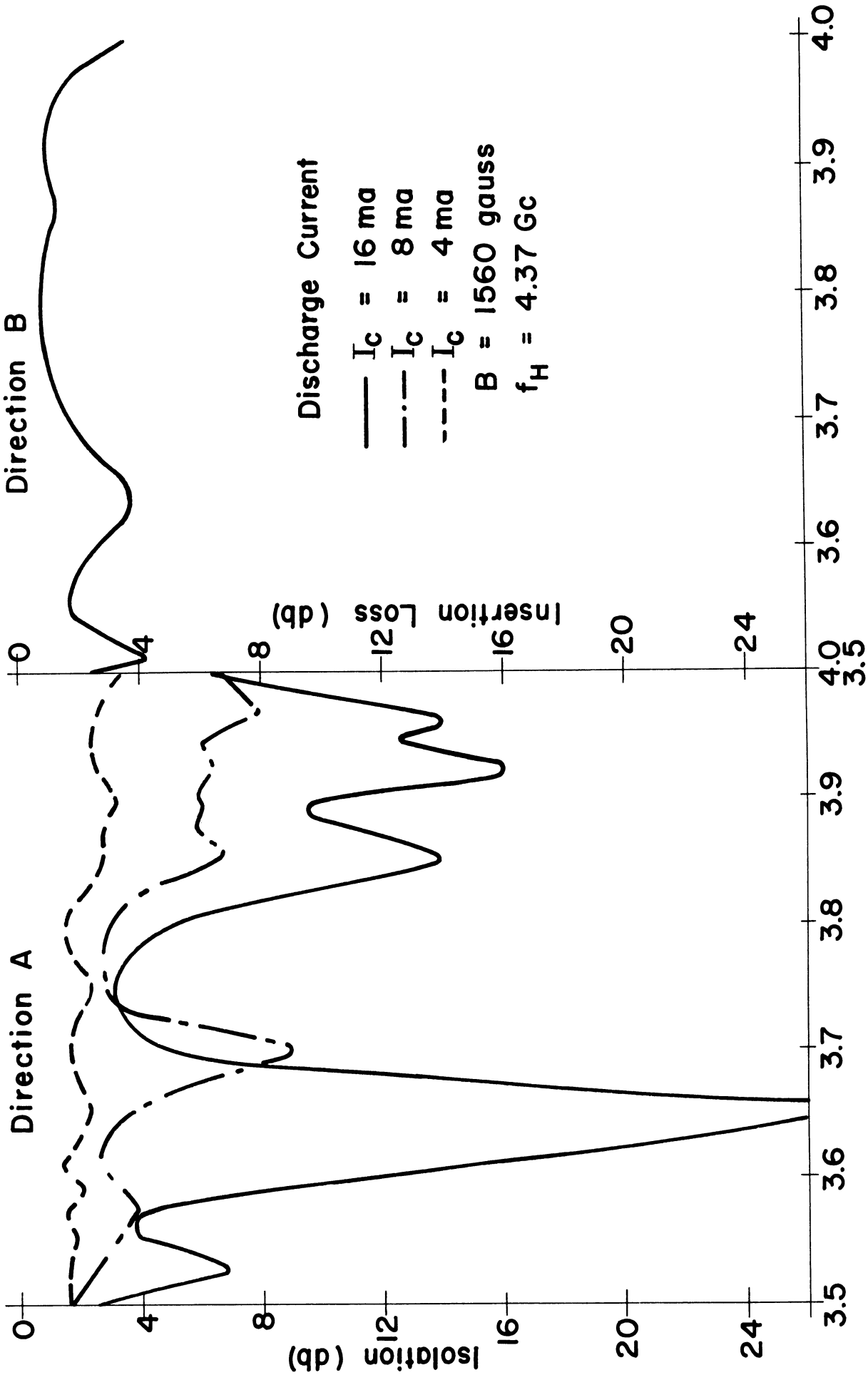

FIG. 3.6: ISOLATION AND INSERTION LOSS VS FREQUENCY FOR VARIOUS DISCHARGE CURRENTS

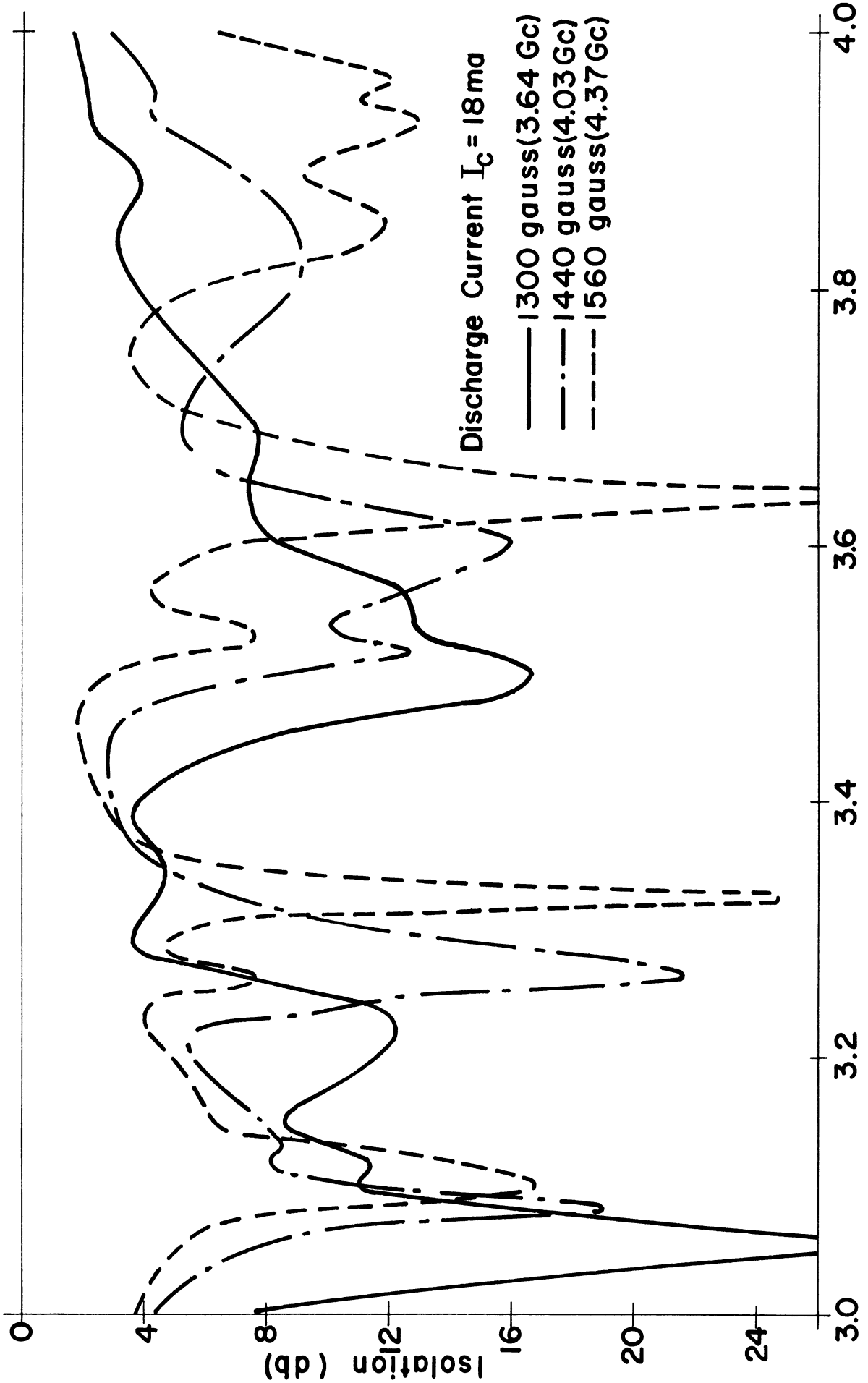

FIG. 3.7: ISOLATION VS FREQUENCY FOR MAGNETIC FIELD STRENGTHS OF 1300, 1440 AND 1560 GAUSS. CORRESPONDING CYCLOTRON FREQUENCIES ARE 3.64, 4.03 AND 4.37 Gc.

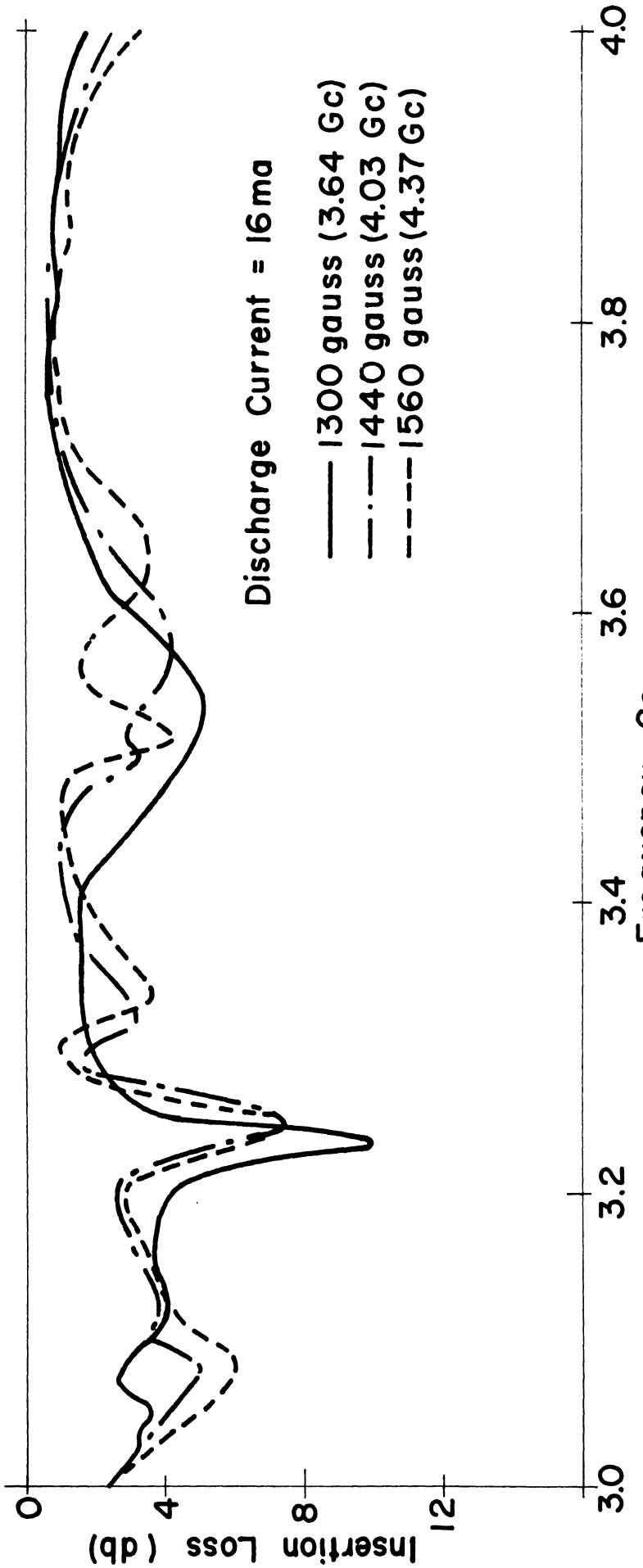

FIG. 3.8: INSERTION LOSS VS FREQUENCY FOR MAGNETIC FIELD STRENGTHS OF 1300, 1440 AND 1560 GAUSS

The data presented in Figures 3.9 and 3.10 lends support to this conclusion. Figure 3.9 shows the isolation, insertion loss and the reflected power, identical for practical purposes, in both directions, without mode suppressors. In Figure 3.10, these quantities are shown with mode suppressors. The discharge current used was 18 to 20 ma and the magnetic field was about 1550 gauss. Addition of the mode suppressors has resulted in eliminating or reducing three of the peaks of Figure 3.9 located at about 3.1, 3.3 and 3.6 Gc, while adding a new peak at about 3.46 Gc. This new peak occurs close to the frequency where a no-plasma resonance is observed and is probably associated with it. These two sets of isolation curves have a similar structure between 3.8 and 4.0 Gc.

3.5 Variable Magnetic Field Characteristics of Isolator.

Because of the difficulty in locating the cyclotron resonance - TM_{11} mode absorption in the presence of other mode conversion resonances, it was felt that it would be informative to examine the isolator RF behavior as the magnetic field is continuously varied. Also, we were interested to see whether the cyclotron absorption could be seen at radio frequencies which are harmonically related to f_H. Bekefi, et al, (Ref. 3.3) have reported seeing this effect as high as the fifth harmonic of f_H.

This experiment was performed after the mode suppressors were added to the isolator. Data was taken for several frequencies with discharge currents ranging from 2.5 to 20 ma. The discharge current was somewhat affected by changing the

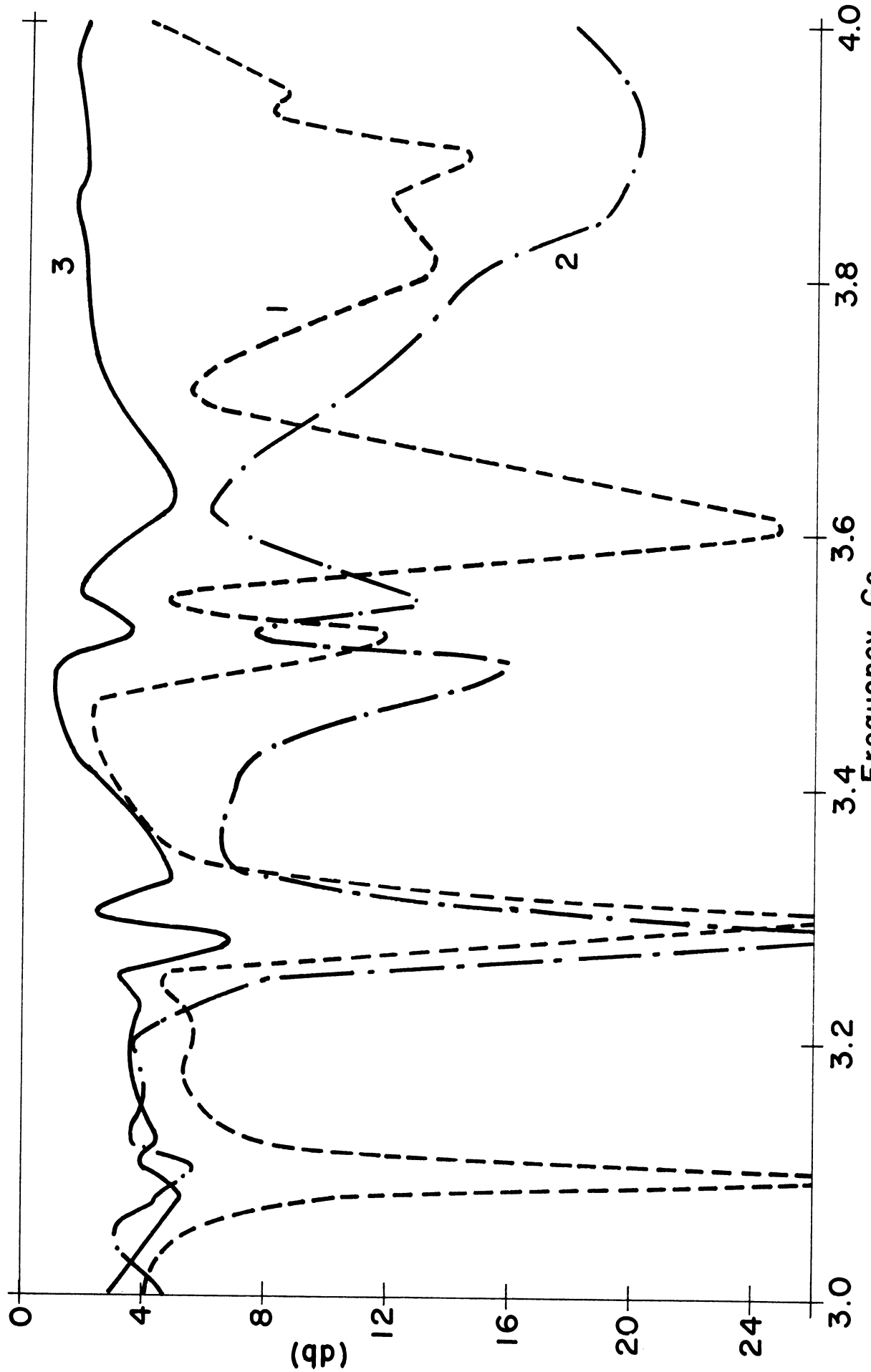

FIG. 3.9: ISOLATION, REFLECTED POWER AND INSERTION LOSS VS FREQUENCY FOR ISOLATION WITHOUT MODE SUPPRESSORS. I_c = 18 ma AND B = 1560 GAUSS

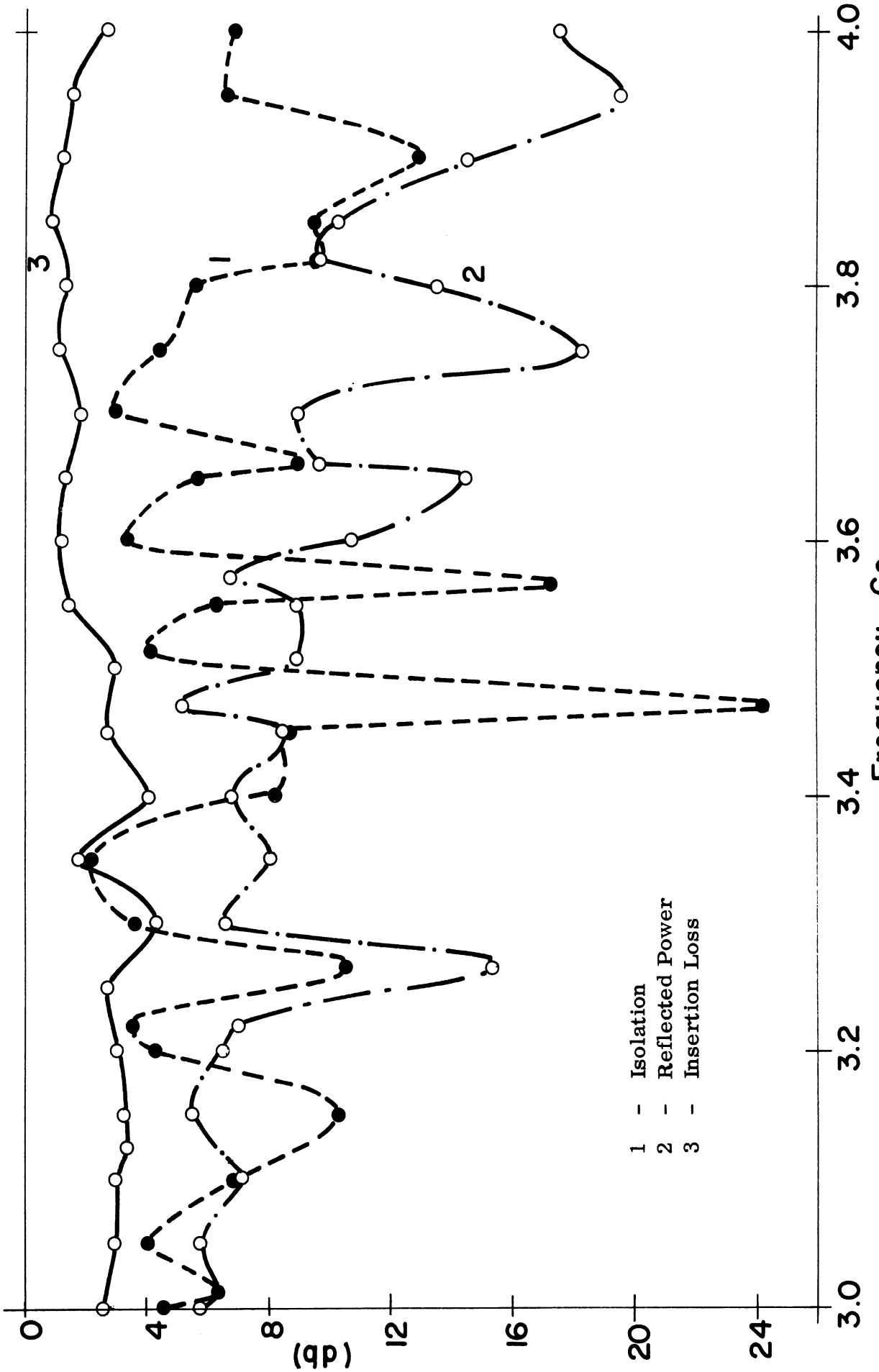

FIG. 3.10: ISOLATION, REFLECTED POWER AND INSERTION LOSS VS FREQUENCY FOR ISOLATION WITH MODE SUPPRESSORS. I_c = 20 AND B = 1550 GAUSS

magnetic field; the variation is about 25 per cent from 0 to 2000 gauss. Values listed in the graphs are those for a field of 1500 gauss.

Figures 3.11 through 3.14 show the isolation, insertion loss and reflected power at a frequency of 3.9 Gc as a function of magnetic field strength. This particular frequency is used here since it falls in a frequency range where the no-plasma insertion loss is free from large resonance effects.

From the isolation and reflection data for direction A (Figures 3.11 and 3.12), it may be seen that a decrease in transmitted power is accompanied by a corresponding increase in the reflected power except for the range between 1400 and 1600 gauss. In other words, the power loss tends to be reactive rather than dissipative except in the latter range. This may lead one to conclude that the cyclotron loss mechanism is causing the decrease of the transmitted power in this range of magnetic fields.

An examination of the insertion loss in Direction B (Fig. 3.13) reveals a structure similar to that for Direction A for magnetic field strength less than 1400 gauss. For the higher discharge currents the structure is also similar for magnetic fields greater than 1600 gauss. The reflected power in direction B (Fig. 3.14) resembles that for Direction A. Also an increase of insertion loss is accompanied by an increased reflected power.

Thus, the transmission and reflection characteristics for the two directions have a qualitative resemblance, except for magnetic field strengths of about 1400 to

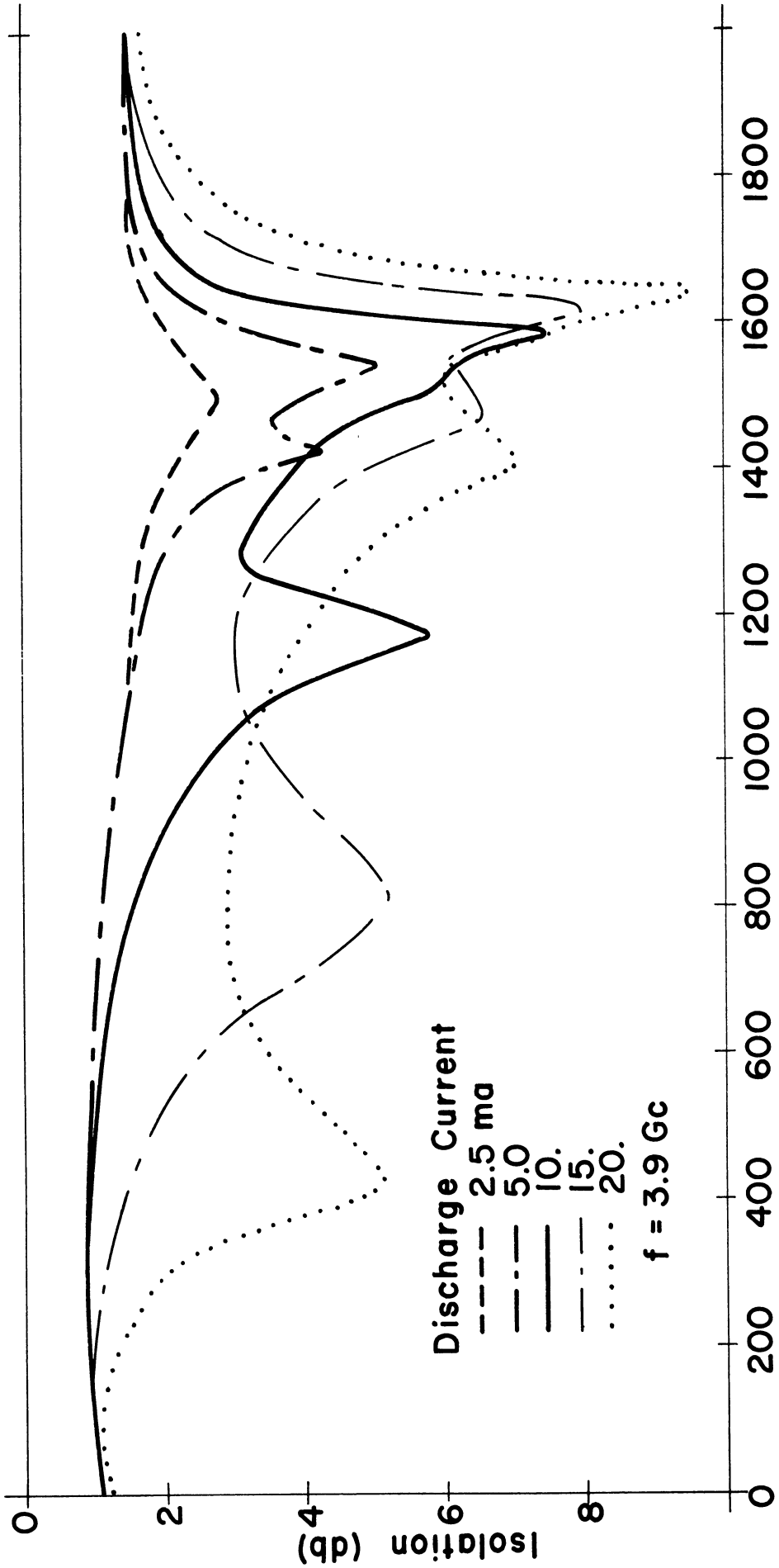

FIG. 3.11: ISOLATION VS MAGNETIC FIELD STRENGTH FOR VARIOUS DISCHARGE CURRENTS AT 3.9 GC

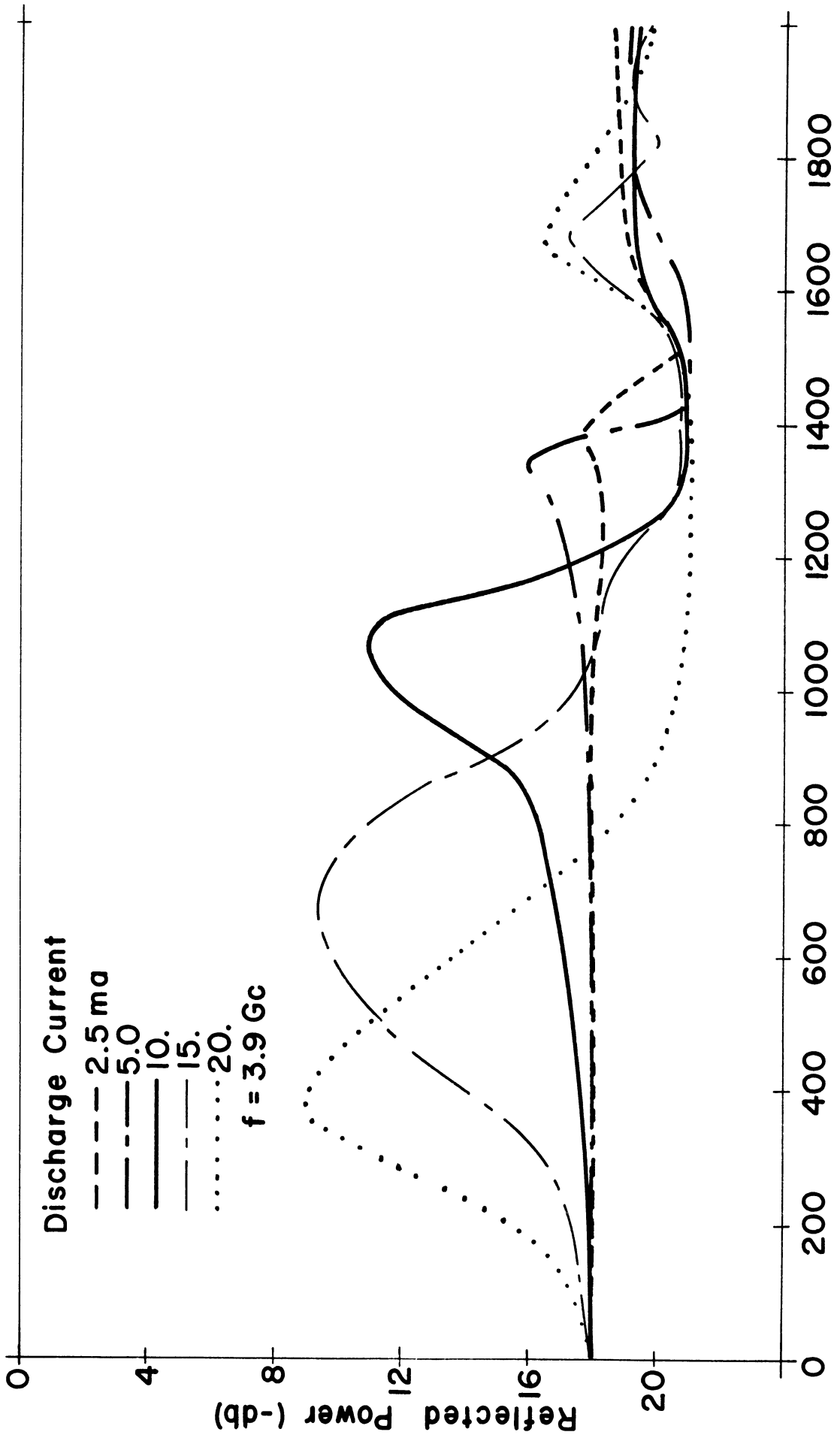

FIG. 3.12: REFLECTED POWER VS MAGNETIC FIELD STRENGTH FOR VARIOUS DISCHARGE CURRENTS AT 3.9 GC, DIRECTION A

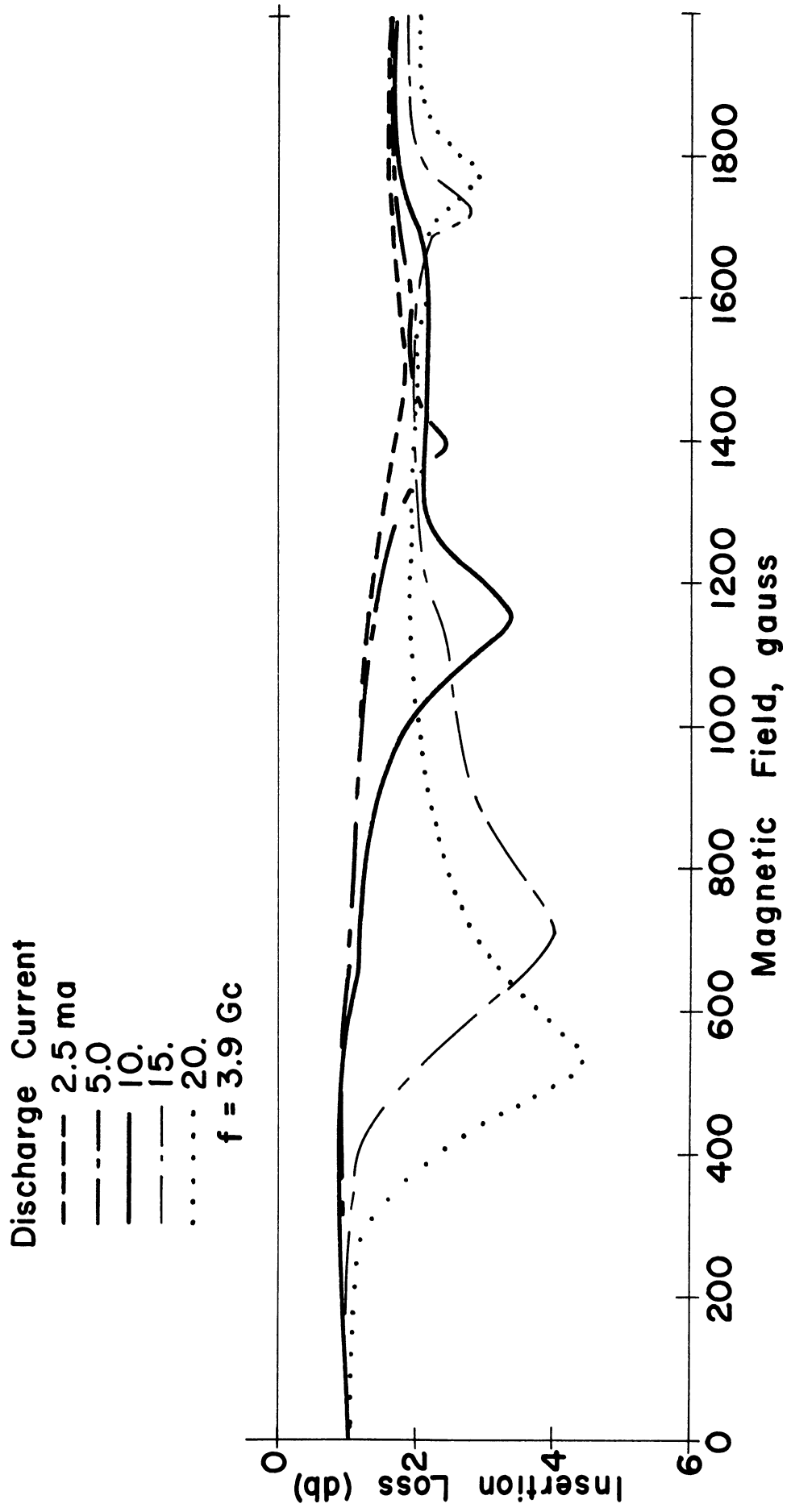

FIG. 3.13: INSERTION LOSS VS MAGNETIC FIELD STRENGTH FOR VARIOUS DISCHARGE CURRENTS AT 3.9 GC

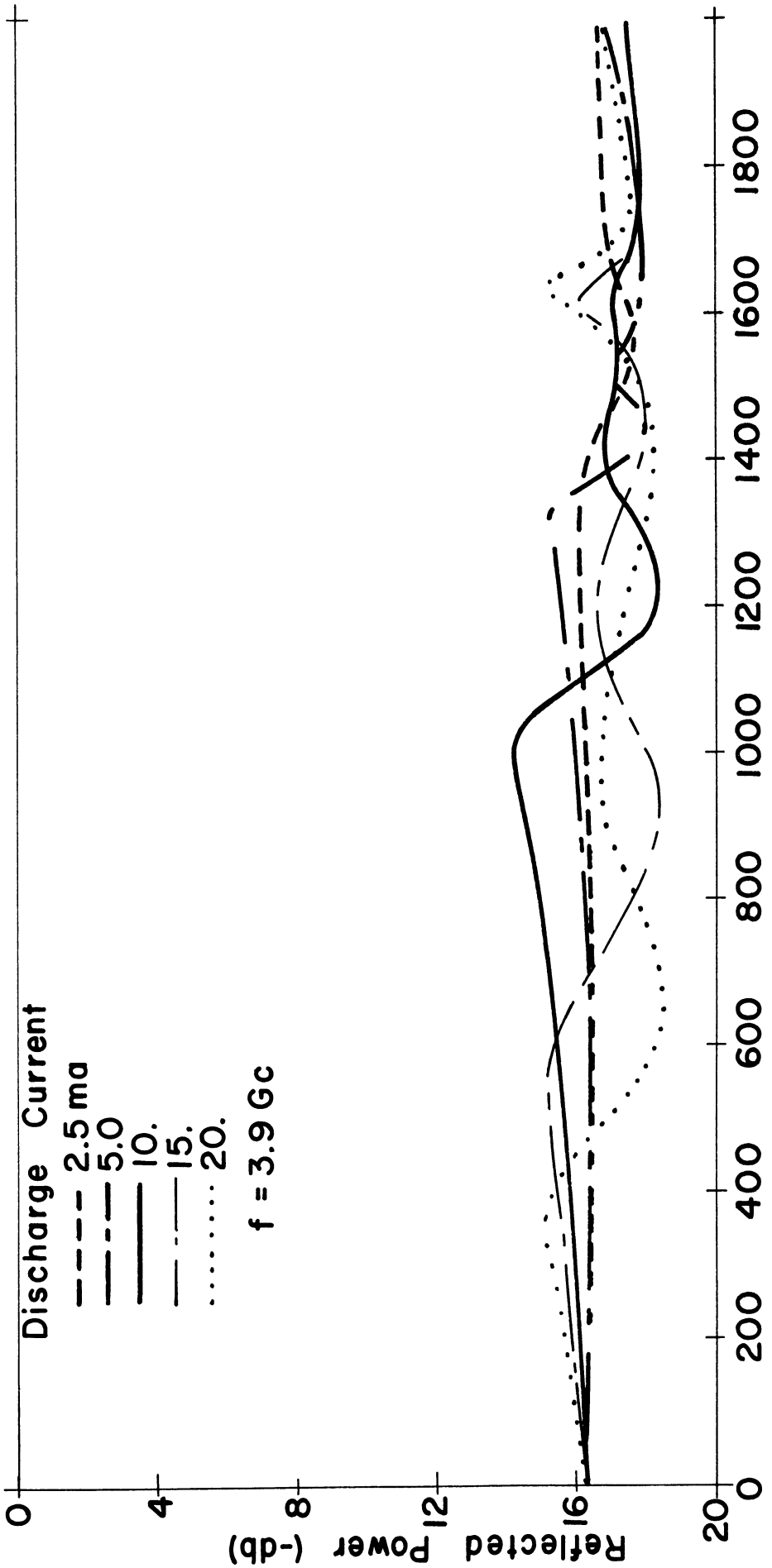

FIG. 3.14: REFLECTED POWER VS MAGNETIC FIELD STRENGTH FOR VARIOUS DISCHARGE CURRENTS AT 3.9 GC, DIRECTION B

1600 gauss. In this region, the transmission curves are distinctly non-reciprocal. This non-reciprocity becomes more evident in the curve of Figure 3.15, where the absorbed power in both directions is plotted for a discharge current of 20 ma.

3.6 Qualitative Analysis of the Data.

Figures 3.16 and 3.17 show the variation in the real and imaginary component of the permittivity for a circularly polarized wave propagating parallel to a magnetic field in an infinite medium. The effective permittivities, ϵ_+ and ϵ_-, corresponding to the extraordinary and the ordinary wave, are given by

$$\epsilon_{\pm}/\epsilon_o = 1 - \frac{(f_p/f)^2}{1 \mp \frac{f_H}{f} + j\frac{\nu_m}{2\pi f}}$$

and

$$\epsilon_{\pm}/\epsilon_o = \frac{\epsilon'_{\pm}}{\epsilon_o} - j\frac{\epsilon''_{\pm}}{\epsilon_o} \quad .$$

In Figure 3.16, f_H is the independent variable and in Figure 3.17, f is the independent variable. The values chosen for the parameters f_p, ν_m and f_H or f, when they are not the independent variable, correspond to the experimental values of these parameters, for some of the data presented in this report. Some understanding of the operation of the plasma resonance isolator may be obtained from these graphs. This is because the isolator plasma electrons are subject to an RF electric field and a static magnetic field in the isolator that are related in the same manner as are the fields in the infinite medium case discussed above.

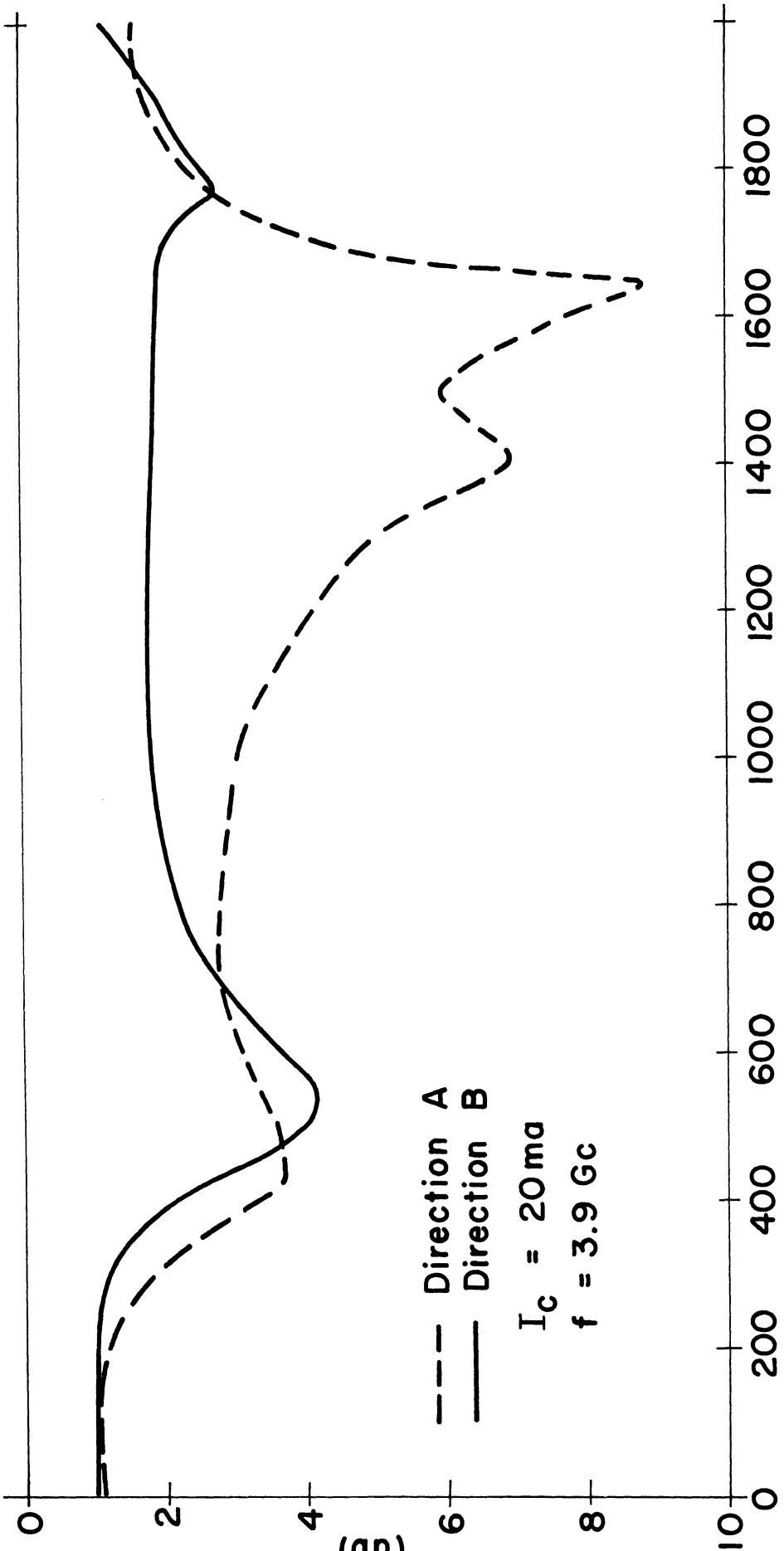

FIG. 3.15: POWER ABSORBED BY ISOLATION IN BOTH DIRECTIONS AS A FUNCTION OF MAGNETIC FIELD STRENGTH

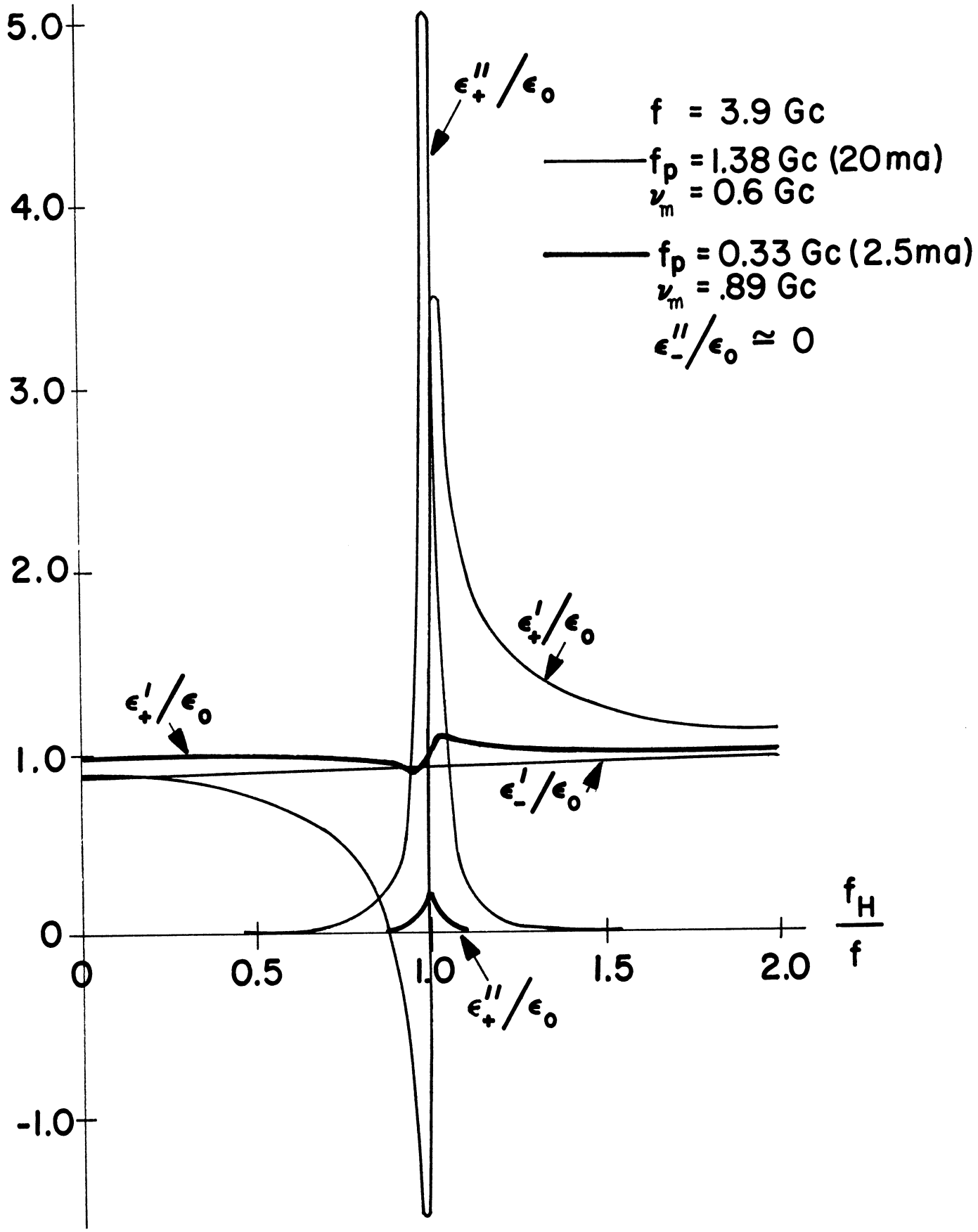

FIG. 3.16: RELATIVE PERMITTIVITY FOR ORDINARY AND EXTRAORDINARY WAVES AS A FUNCTION OF CYCLOTRON FREQUENCY

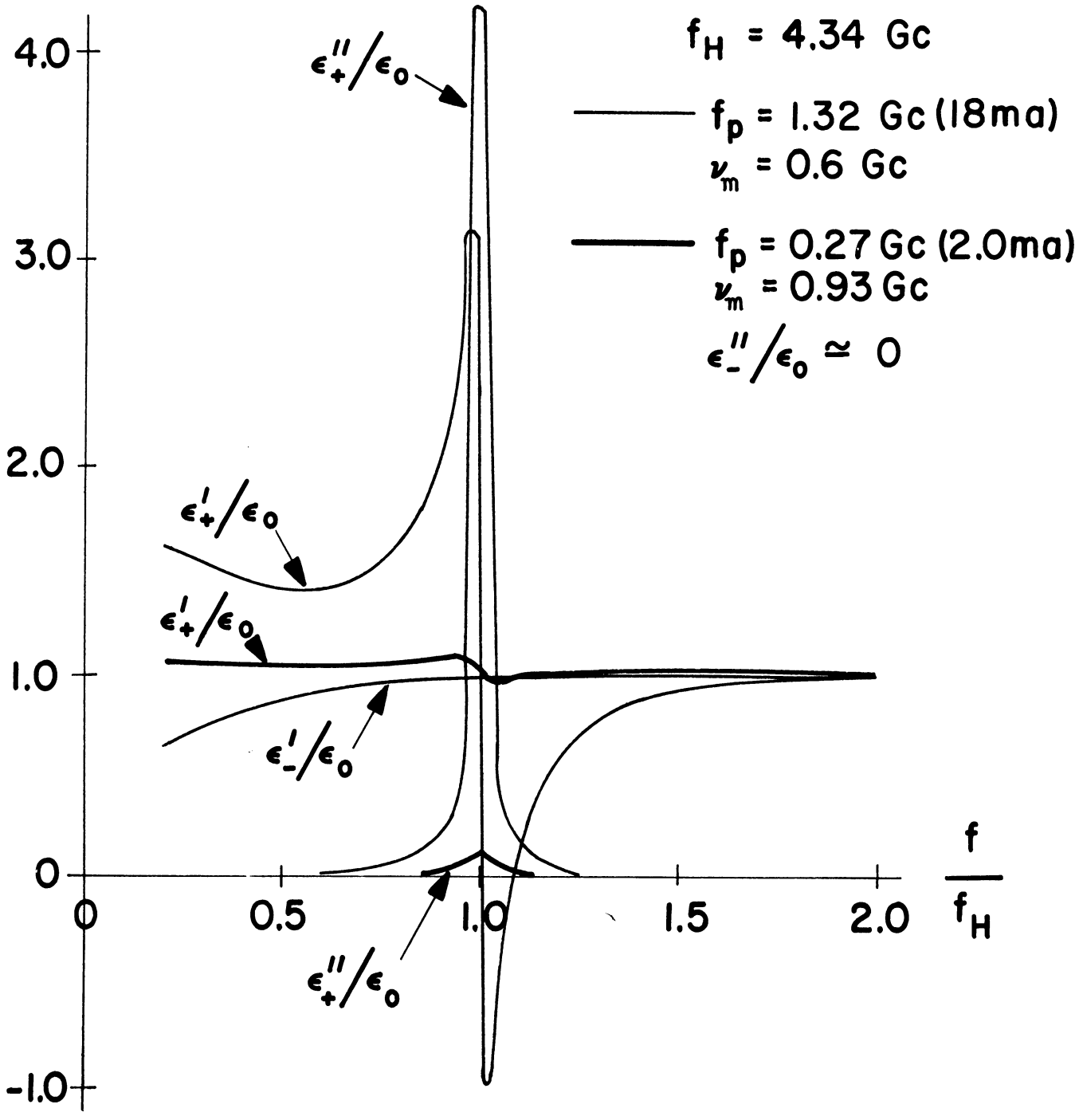

FIG. 3.17: RELATIVE PERMITTIVITY FOR ORDINARY AND EXTRAORDINARY WAVES AS A FUNCTION OF MICROWAVE FREQUENCY

First, note that ϵ''_-/ϵ_o, the imaginary part of the permittivity of the ordinary wave is negligible for all cases in the experiment and that ϵ'_-/ϵ_o is little different from unity. This means that the propagation characteristic in direction B should be unaffected by the magneto-plasma. Second, observe that for the extraordinary wave the real and imaginary parts of the permittivity, ϵ_+/ϵ_o, vary considerably, especially for the higher plasma frequency curve considered.

Consider Figure 3.16 more closely now, where f_H is the independent variable. The parameter values here correspond to the data shown in Figure 3.11 for discharge currents of 2.5 and 20 ma, and f = 3.9 Gc. ϵ''_+/ϵ_o has a maximum value where f_H = f, which in this case would be 3.9 Gc. One should then expect the maximum absorption to occur close to f_H = 3.9 Gc. As implied by the graph an appreciable absorption might be expected over a range of f_H/f of approximately 0.8 to 1.2, for a discharge current of 20 ma. The experimental data of Figure 3.11 shows that the maximum absorption occurs at magnetic field values corresponding to cyclotron frequencies between 3.9 and 4.5 Gc.

Now consider Figure 3.17 where the parameter values for the plasma frequency correspond to a discharge current of 2.0 ma and 18 ma with B = 1560 gauss. Experimental data with these plasma frequency and magnetic field values is shown in Figures 3.6 and 3.7. Again we find that ϵ''_+/ϵ_o has a maximum value at $f = f_H$. The curve indicates that the absorption should be expected to decrease fairly

rapidly as f/f_H is varied about unity. Qualitatively, one might expect to see absorption over a range of f/f_H of approximately 0.8 to 1.1 for a discharge current of 20 ma. Recognition of a cyclotron peak in the data of Figures 3.6 and 3.7 is made difficult by the various resonance peaks which occur in this frequency interval.

Let us now make an estimate of the width of the absorption region in either magnetic field strength (when f_H is the independent variable) or microwave frequency (when f is the independent variable) as implied by Figures 3.16 and 3.17. We estimated from the curves of ϵ''_+/ϵ_o in Figure 3.16 that a region of appreciable absorption might occur for $0.8 \lesssim f_H/f \lesssim 1.2$. At a frequency of 3.9 Gc, then, f_H ranges between 3.1 to 4.7 Gc, or B between 1120 to 1670 gauss. From Figure 3.17, for a magnetic field of 1560 gauss (4.34 Gc), the estimated RF absorption region would be from 3.5 to 4.8 Gc.

These results are enlightening. They indicate that the energy loss due to the cyclotron resonance mechanism may occur over a fairly wide interval about $f = f_H$. In a realistic situation, where the magnetic field is not uniform over the plasma volume, the effect would be to further widen the absorption interval. In addition, as the absorption bandwidth increases, one would expect that the maximum absorption would decrease.

To summarize, we can make these observations:

(1) The magnetic field used in this experiment varied over the plasma

volume to $\pm$ 10 to 15 per cent. At a field strength of 1500 gauss, a minimum variation of 300 gauss or a variation in f_H of 840 Mc may be expected over the plasma volume. This would widen the absorption region while decreasing the maximum absorption.

(2) Asymmetries in the isolator result in mode conversion, i.e. energy in the TM_{11} mode is changed to a non-symmetric mode. This energy is effectively absorbed by the square waveguide section walls since it cannot re-enter the coaxial line.

(3) Experimentally, the isolator exhibits a very strong non-reciprocity in transmission characteristics. High Q non-reciprocal resonance absorption regions of greater than 30 db directivity occur. The frequency at which they occur has no well-determined relation to magnetic field strength. They seem rather to be related to resonant frequencies in the chamber.

(4) The features of the direct cyclotron resonance absorption in the isolator are obscured by the mode conversion resonance effects.

3.7 Conclusions

The above discussions lead us then to the following conclusions concerning the isolator operation:

(1) The most important loss mechanism in the non-reciprocal transmission characteristic of the isolator is mode conversion. Propagation in direction B is

largely unaffected by the magneto-plasma since the plasma permittivity as seen by the longitudinal electric field of the TM_{11} mode differs negligibly from that of free space therefore maintaining the waveguide symmetry. In direction A, however, the permittivity varies considerably from that of free space, producing a non-symmetric waveguide.

(2) Loss of incident energy directly out of the TM_{11} mode to the cyclotron resonance absorption was degraded by the inhomogeneous static magnetic field and the mode conversion resonance effects. The magnetic field swept data seems to offer the best opportunity to observe directly electron cyclotron resonance absorption.

REFERENCES FOR SECTION III

3.1 S. Ramo and J. R. Whinnery, Fields and Waves in Modern Radio, John Wiley and Sons (1950 and 1960).

3.2 A. Olte and K. M. Siegel "Distinction Between the Electromagnetic Constants of Tektites and Libyan Desert Glass and Their Effect on Lunar Surface Theory," Astrophysical J., Vol. 133, No. 2, 706-717 (March 1961).

3.3 G. Bekefi, J. D. Coccoli and E.B.Hooper, Jr., "Microwave Emission and Absorption at Cyclotron Harmonics of a Warm Plasma," Phys. Rev. Ltrs. Vol. 9, No. 1, 6-9(July 1962).

IV

CONCLUSIONS

The use of plasmas in microwave applications has been investigated. It was reconfirmed that components such as the coaxial variable attenuator and switch using plasmas may be potentially feasible. It appears that one must depend on local ionization of the gas to control the microwaves. It is not very easy to achieve linear attenuation with this mechanism. Not much success was achieved with diffusion of plasmas by application of voltage gradients. A microwave isolator employing a magneto-plasma was investigated experimentally. A very significant isolation was obtained by the non-reciprocal mode conversion. As a result the principal mode-cyclotron resonance absorption which was observed was less than anticipated. The sensitive dependence of the non-reciprocal mode conversion on the discharge current may offer a mechanism for designing a microwave limiter.

The primary difficulty in designing useful plasma-microwave circuits is not the inadequady of the microwave theory, but rather that we do not have available today a convenient and stable plasma package. One uses ideas and techniques for generation of plasmas that were developed for other applications where the stability requirements are not as critical, and package size may be entirely left to convenient choices. The production and control of plasmas for microwave applications thus constitutes an area where further work is highly necessary. If a suitably packaged plasma with a reasonable stability were available, plasma devices seem particularly

promising in areas where the solid state and ferrite devices have serious drawbacks, such as for high temperature applications.